PHYSICAL REVIEW D **81,** 113011 (2010)

Electromagnetic form factors of the Δ with D-waves

G. Ramalho,[1,2] M. T. Peña,[2,3] and Franz Gross[1,4]

[1]*Thomas Jefferson National Accelerator Facility, Newport News, Virginia 23606, USA*
[2]*Centro de Física Teórica de Partículas, Av. Rovisco Pais, 1049-001 Lisboa, Portugal*
[3]*Department of Physics, Instituto Superior Técnico, Av. Rovisco Pais, 1049-001 Lisboa, Portugal*
[4]*College of William and Mary, Williamsburg, Virginia 23185, USA*

(Received 24 February 2010; published 30 June 2010)

The electromagnetic form factors of the Δ baryon are evaluated within the framework of a covariant spectator quark model, where S- and D-states are included in the Δ wave function. We predict all the four Δ multipole form factors: the electric charge G_{E0}, the magnetic dipole G_{M1}, the electric quadrupole G_{E2} and the magnetic octupole G_{M3}. We compare our predictions with other theoretical calculations. Our results are compatible with the available experimental data and recent lattice QCD data.

DOI: 10.1103/PhysRevD.81.113011 PACS numbers: 13.40.Gp, 12.38.Gc, 12.39.Ki, 14.20.Gk

I. INTRODUCTION

In the history of hadronic physics the nucleon was one of the first particles to have its internal structure experimentally uncovered. The nonpointlike character of the nucleon was suggested by the measurements of the proton anomalous magnetic moment. Around 1950, measurements disclosed an exponential falloff for the charge distribution, and three decades later the SLAC measurements showed that the corresponding charge form factor in momentum space coincided, almost perfectly, with the magnetic dipole form factor. This image of the proton proved to be a good approximation for low Q^2, the square of the four-momentum transfer, and was only superseded by the results from the Jlab polarization measurement in 1999 [1].

The study of the next baryonic state (the Δ) has been more challenging. Although the pure spin $3/2$ and isospin $3/2$ structure of the Δ was clearly isolated from the background of the pion nucleon scattering experimental cross sections, its theoretical description is not yet totally clear. Quantum chromodynamics (QCD) emphasizes the three-quark state component, and historically the existence of the Δ^{++} led to the introduction of color as a quantum number. Still, the issue on how much of the Δ structure comes from a three-quark state, and how much is a molecularlike state of a nucleon and a pion, remains an open question.

Since the Δ is a spin $3/2$ particle, its electromagnetic structure can be characterized by four form factors, namely, the electric charge G_{E0}, magnetic dipole G_{M1}, the electric quadrupole G_{E2} and electric octupole G_{M1} form factors. The first two describe the charge and magnetic dipole distributions, while the last two measure the deviation of the first ones from the symmetric form [2]. At zero transferred momentum squared, $Q^2 = 0$, the form factors define the Δ multipole moments: the charge e_Δ, the magnetic moment μ_Δ, the electric quadrupole moment Q_Δ and the magnetic octupole moment $\mathcal{O}_\Delta$. If the Δ would simply be a completely symmetric state, with no quark D-states relatively to the quark pair (diquark), both Q_Δ and $\mathcal{O}_\Delta$ would vanish [3].

The unstable character of the Δ (with a mean lifetime of 5.6×10^{-24} s) makes it difficult to probe the electromagnetic properties of this particle/resonance. Until recently the available information on the Δ structure came from the study of the $\gamma N \rightarrow \Delta$ reaction only. The dominance of the magnetic dipole moment in that reaction asserts the spin flip of a quark in the nucleon as the main process, but the magnitudes of the quadrupole contributions (G_E^* and G_C^*) indicate a small deformation of the Δ [4].

The experimental information on the Δ is restricted to the Δ^{++} and Δ^{+} magnetic moments [5–12]. Even so, those results are affected by considerable error bars, due to the unstable nature of the Δ and theoretical model uncertainties. This is particularly true for the Δ^{+} magnetic moment [6]. See Refs. [7,12] for a review. New experiments are in progress at MAMI [12] to extract μ_{Δ^+} more accurately with the help of reaction models based on hadronic degrees of freedom [11,13,14]. The scarce experimental information on μ_Δ is compensated by extensive theoretical studies within various frameworks [11,14–50]. For a review see Ref. [3]. As for other Δ observables, there is no other information, with the exception of the electric quadrupole moment Q_Δ, which was estimated using a connection to the $\gamma N \rightarrow \Delta$ transition quadrupoles [51]. For $Q^2 \neq 0$ there is no experimental information related to the Δ form factors. Even a very basic property like the Δ electric charge radius is at present rather unknown, contrarily to what happens for the nucleon, where that quantity is accurately measured [52]. Our knowledge on the Δ charge radius relies so far only on diverse theoretical model calculations [28,31,33,43,45,53–62]. There are also theoretical calculations of the Δ quadrupole moment Q_Δ [28,30,31,33,49,60–72].

Recently, the nature of the Δ was explored in another direction, and under another light. Lattice QCD, the discrete version of the fundamental nonperturbative theory of the hadrons, was used to estimate the Δ elastic form factors [73–76], following the pioneer works of Bernard *et al.* [77] and Leinweber *et al.* [78]. The works [73,76,78] are based

on the quenched approximation. The works [74,75] are unquenched calculations, which include also sea quark effects. The results of the MIT-Nicosia group [73–75] were obtained for a wide range of Q^2, while the calculations of the Adelaide group [76] are performed for only one small value of Q^2 (the limit case $Q^2 = 0$ is impossible to reach for technical reasons) and extrapolated for $Q^2 = 0$ to obtain the Δ multipoles and the charge and magnetic radii. In particular for $Q^2 = 0$ the background field method was used to calculate with a good accuracy the Δ magnetic moment [77,79,80]. These methods were applied to pion mass values within the 0.3–1 GeV region and consequently some extrapolations are required [14,81]. In the absence of direct experimental information lattice QCD provides the best reference for theoretical calculations for finite Q^2.

Motivated by the recent publication of lattice QCD data for the Δ form factors [73–76,80], several models were also extended to determine those physical quantities. Calculations of the Δ form factors were performed within the covariant spectator theory [3,82] and also within a chiral quark-soliton model (χQSM) [62]. Also, the magnetic octupole moment $\mathcal{O}_\Delta$ was estimated by Buchmann [2], using a deformed pion cloud model, and by Geng [49], using χPT. Both $\mathcal{Q}_\Delta$ and $\mathcal{O}_\Delta$ were estimated using QCD sum rules [69] and a covariant spectator quark model [82].

In this work we use a constituent quark model based on the covariant spectator formalism [4,83–85] to predict the Q^2 dependence of all four Δ multipole form factors. Our results will be compared with the available experimental data, and the results from other models in the literature, as well as with recent lattice data. The Δ electromagnetic form factors give us an insight into the Δ internal structure. In particular the determination of the Δ electric quadrupole and magnetic octupole moments gives information on how the Δ is deformed, and on its size and shape. And this information is valuable, as we will conclude, to adequately constrain quark models. These in turn can be used to extrapolate and interpret lattice results.

The nucleon, as a spin $1/2$ particle, has no electrical quadrupole moment, and the Δ, a spin $3/2$ state, emerges as the first candidate for a deformed baryon. A deformation (compression or expansion along the direction of the spin projection) would imply $\mathcal{Q}_\Delta \neq 0$. The interpretation of $\mathcal{Q}_\Delta \neq 0$ as a signature of distortion matches well with our intuitive notion of deformation, based on the nonrelativistic limit of the Breit frame form factors. In that limit the Fourier transformation of the form factors gives the spatial distribution of charge or magnetic moment. We will therefore identify this notion as *classical deformation*. Recently, an alternative interpretation of distortion, based on transverse densities defined in the infinite moment frame, was introduced by other authors [75,86–88]. Our calculations in this paper provide the basis needed for a forthcoming analysis of the Δ deformation under the *classical* perspective and also in the newer perspective [89].

It is clear that the study of the Δ form factors is a very interesting topic, even if experimentally arduous. The only experimental source of information about the Δ deformation comes today from the $\gamma N \to \Delta$ quadrupole transition. However, this reaction depends on orbital angular momentum components in *both* the nucleon and of the Δ [68,90]. It is then very important to have an independent estimate of the angular momentum components in the Δ (leading to a deformation) [74,75,91]. This is the main motive for our focus in this paper on the direct $\gamma\Delta \to \Delta$ reaction.

In our previous work a first covariant spectator constituent quark model was developed for the nucleon, the $\gamma N \to \Delta$ transition and the Δ [4,83–85,92,93]. In the covariant spectator quark model a baryon is described as a system of three constituent quarks, with a off-shell quark free to interact with a electromagnetic field, while the quark pair (diquark) acts as a spectator on-shell particle. Confinement is described effectively, with a quark-diquark vertex assumed to have a zero at the singularity of the three-quark propagator. The quarks are dressed, having an electromagnetic form factor with a behavior consistent with vector meson dominance. Within this first model we calculated the Δ form factors considering the Δ wave function parameterized simply by an S-wave state for the quark-diquark system. In this case only G_{E0} and G_{M1} have nonzero contributions because of the symmetry assumed for the system. In the work reported here we extend the previous model to the inclusion of the D-states, following Ref. [4]. It becomes then possible to predict, without further parameter fitting, nonzero results also for G_{E2} and G_{M3}. Although our results regard only the valence quark contributions, they compare well with a variety of lattice QCD data, besides the available experimental data.

We organize this paper in the following main sections: In Sec. II we introduce the basic definitions used to calculate the Δ electromagnetic form factors. In Sec. III we review the covariant spectator quark model and present the Δ wave function. In Sec. IV we derive the Δ form factors within our model. In Sec. V we show the numerical results. Finally, in Sec. VI we draw some conclusions.

II. Δ ELECTROMAGNETIC FORM FACTORS

The interaction of a photon with an on-mass-shell Δ isobar, with initial four-momentum P_- and final four-momentum P_+, can be parameterized in terms of the electromagnetic current [90,94]:

$$J^\mu = -\bar{w}_\alpha(P_+)\Big\{\Big[F_1^*(Q^2)g^{\alpha\beta} + F_3^*(Q^2)\frac{q^\alpha q^\beta}{4M_\Delta^2}\Big]\gamma^\mu + \Big[F_2^*(Q^2)g^{\alpha\beta} + F_4^*(Q^2)\frac{q^\alpha q^\beta}{4M_\Delta^2}\Big]\frac{i\sigma^{\mu\nu}q_\nu}{2M_\Delta}\Big\}w_\beta(P_-), \tag{1}$$

where M_Δ is the Δ mass, w_α is the Rarita-Schwinger spin $3/2$ state, $F_1^*(0) = e_\Delta$, with $e_\Delta = 0, \pm 1, +2$ the four

possible Δ charge values. The four functions F_i^* $(i = 1, \ldots, 4)$ of Q^2 define the four Δ form factors [in Appendix A, we discuss the general form of (1)]. They can be combined to form the two electric and two magnetic multipoles, which have a direct physical interpretation: the electric charge (E0) and quadrupole (E2), and the magnetic dipole (M1) and octupole (M3) form factors, defined as [3,90,94]

$$G_{E0}(Q^2) = [F_1^* - \tau F_2^*]\left(1 + \frac{2}{3}\tau\right) - \frac{1}{3}[F_3^* - \tau F_4^*]\tau(1+\tau), \tag{2}$$

$$G_{M1}(Q^2) = [F_1^* + F_2^*]\left(1 + \frac{4}{5}\tau\right) - \frac{2}{5}[F_3^* + F_4^*]\tau(1+\tau), \tag{3}$$

$$G_{E2}(Q^2) = [F_1^* - \tau F_2^*] - \frac{1}{2}[F_3^* - \tau F_4^*](1+\tau), \tag{4}$$

$$G_{M3}(Q^2) = [F_1^* + F_2^*] - \frac{1}{2}[F_3^* + F_4^*](1+\tau), \tag{5}$$

where the dimensionless factor

$$\tau = \frac{Q^2}{4M_\Delta^2} \tag{6}$$

was introduced. The static magnetic dipole (μ_Δ), electric quadrupole (Q_Δ) and magnetic octupole ($\mathcal{O}_\Delta$) moments are defined in the $Q^2 = 0$ limit, as

$$\mu_\Delta = \frac{e}{2M_\Delta} G_{M1}(0), \qquad Q_\Delta = \frac{e}{M_\Delta^2} G_{E2}(0), \qquad \mathcal{O}_\Delta = \frac{e}{2M_\Delta^3} G_{M3}(0). \tag{7}$$

III. DELTA WAVE FUNCTIONS

In our model the Δ wave function is described by an mixture of an S-state and two D-state components for the quark-diquark system

$$\Psi_\Delta = N[\Psi_S + a\Psi_{D3} + b\Psi_{D1}], \tag{8}$$

where a and b are, respectively, the admixture coefficients for the two D-states: D3 (quark core spin 3/2) and D1 (quark core spin 1/2). N is the normalization constant. To characterize Ψ_Δ we took the covariant spectator theory for a quark and a on-mass-shell diquark system, as proposed in Ref. [4].

From its symmetry properties, the $J = 3/2$ quark-diquark S-state (quark core $\mathcal{S} = 3/2$ and orbital angular momentum $L = 0$) has the general form

$$\Psi_S(P,k) = -\psi_S(P,k)(T \cdot \xi^{1*})\varepsilon_P^\alpha w_\alpha(P) \tag{9}$$

as proposed in Refs. [4,84]. In this equation ψ_S is a scalar function describing the momentum distribution of the quark-diquark system in terms of the Δ and the diquark moment, P and k, respectively; ε_P^* is the polarization state associated with the diquark spin [92] (the polarization index was omitted in this short-hand notation) and w_β is the Rarita-Schwinger state. The isospin-$\frac{3}{2}$ to isospin-$\frac{1}{2}$ transition operators are represented by T_i $(i = x, y, z)$ [3,14,84,90], and $\xi^{1*}(I_z)$ is the spin-1 diquark state (a combination of u and d quarks). The isospin operator $(T \cdot \xi^{1*})$ acts on the Δ isospin states. (See Ref. [84] for details.) The normalization of the wave function (9) to unity implies for the scalar wave function the normalization condition

$$\int_k [\psi_S(\bar{P}, k)]^2 = 1, \tag{10}$$

where $\bar{P} = (M_\Delta, 0, 0, 0)$ and the covariant integral over the momentum k is defined in Eq. (25) below.

The Δ D-states in the spectator formalism were introduced and explained in detail in Ref. [4]. Their definition is made through the $\mathcal{D}$-state operator defined as

$$\mathcal{D}^{\alpha\beta}(P_\pm, k_\pm) = \tilde{k}_\pm^\alpha \tilde{k}_\pm^\beta - \frac{\tilde{k}_\pm^2}{3}\tilde{g}_\pm^{\alpha\beta}, \tag{11}$$

where

$$\tilde{k}_\pm^\alpha = k^\alpha - \frac{P_\pm \cdot k}{M_\Delta^2} P_\pm^\alpha \tag{12}$$

is the covariant generalization of the three-momentum in Δ rest frame, and

$$\tilde{g}_\pm^{\alpha\beta} = g^{\alpha\beta} - \frac{P_\pm^\alpha P_\pm^\beta}{M_\Delta^2} \tag{13}$$

generalizes the unity operator. The variables P_- (P_+) describe the initial (final) momentum, and in the same way $\tilde{k}_-$ $(\tilde{k}_+)$ refer to the initial (final) state.

Using the operator $\mathcal{D}$ a generic spin 3/2 D-state is

$$\mathcal{W}^\alpha(P,k;\lambda) = \mathcal{D}^{\alpha\beta}(P,k) w_\beta(P,\lambda). \tag{14}$$

It decomposes into a sum of two D-states, associated with the two possible spin states of the quark core, $\mathcal{S} = 1/2$ or $\mathcal{S} = 3/2$ (core-spin states). To separate the two core-spin states we consider the two projection projectors:

$$(\mathcal{P}_{1/2})^{\alpha\beta} = \frac{1}{3}\tilde{\gamma}^\alpha \tilde{\gamma}^\beta, \tag{15}$$

$$(\mathcal{P}_{3/2})^{\alpha\beta} = \tilde{g}^{\alpha\beta} - \frac{1}{3}\tilde{\gamma}^\alpha \tilde{\gamma}^\beta, \tag{16}$$

where

$$\tilde{\gamma}^\alpha = \gamma^\alpha - \frac{\not{P} P^\alpha}{M_\Delta^2}. \tag{17}$$

The properties of the core-spin projectors are known in the literature [95,96].

The amplitudes for the states associated to the core-spin $\mathcal{S} = 1/2$ (D1-state) and $\mathcal{S} = 3/2$ (D3-state) are defined as

$$\Psi_{D1}(P,k) = -3\psi_{D1}(T\cdot\xi^{1*})\varepsilon^{\alpha*}_{\lambda P}W_{D1\alpha}(P,k), \quad (18)$$

$$\Psi_{D3}(P,k) = -3\psi_{D3}(T\cdot\xi^{1*})\varepsilon^{\alpha*}_{\lambda P}W_{D3\alpha}(P,k), \quad (19)$$

where

$$W_{D1\alpha}(P,k;\lambda_\Delta) = (\mathcal{P}_{1/2})_{\alpha\beta}\mathcal{W}^\beta(P,k;\lambda_\Delta), \quad (20)$$

$$W_{D3\alpha}(P,k;\lambda_\Delta) = (\mathcal{P}_{3/2})_{\alpha\beta}\mathcal{W}^\beta(P,k;\lambda_\Delta). \quad (21)$$

As before, $(T\cdot\xi^{1*})$ acts on the Δ isospin states. For simplicity, in our notation the diquark polarization (λ) and Δ spin projections (λ_Δ) are suppressed in the wave functions. Also $\psi_{D1} = \psi_{D1}(P,k)$, $\psi_{D3} = \psi_{D3}(P,k)$ are scalar wave functions. The factor -3 was introduced for convenience. The normalization of the wave functions is

$$\int_k \{\tilde{k}^4[\psi_{D2S}(\bar{P},k)]^2\} = 1, \quad (22)$$

and ensures that the wave function Ψ_Δ satisfies the charge condition,

$$3\sum_\lambda \int_k \bar{\Psi}_\Delta(\bar{P},k)j_1(0)\gamma^0\Psi_\Delta(\bar{P},k) = e_\Delta. \quad (23)$$

The variable $\bar{P}$ represents $P = P_+ = P_-$ in the Δ rest frame ($Q^2 = 0$) and $j_1(0) = \frac{1}{6} + \frac{1}{2}\tau_3$ is the (quark) charge operator at $Q^2 = 0$. See Ref. [4] for more details about the D-states.

IV. CURRENT AND FORM FACTORS

Within the covariant spectator theory, the electromagnetic current in impulse approximation, can be written as in Refs. [4,83,84]

$$J^\mu = 3\sum_\lambda \int_k \bar{\Psi}_\Delta(P_+,k)j_I^\mu\Psi_\Delta(P_-,k), \quad (24)$$

which sums in all intermediate diquark polarization and integrates over the diquark three-momentum

$$\int_k \equiv \int \frac{d^3k}{(2\pi)^3 2E_k}. \quad (25)$$

It also includes the symmetrization of the quark current. Following Ref. [83] the photon-quark interaction is represented by

$$j_I^\mu = \left(\frac{1}{6}f_{1+} + \frac{1}{2}f_{1-}\tau_3\right)\gamma^\mu + \left(\frac{1}{6}f_{2+} + \frac{1}{2}f_{2-}\tau_3\right)\frac{i\sigma^{\mu\nu}q_\nu}{2M_N}, \quad (26)$$

where M_N is the nucleon mass and the isospin (τ_3) and spin (γ^μ) operators acts on the Δ initial and final states. The coefficients $f_{i\pm}$ with $i = 1, 2$ are the quark form factors and function of Q^2. The explicit form of $f_{i\pm}$ will be introduced later in Sec. V.

For numerical applications we define the isospin dependent functions $\tilde{e}_\Delta$ and $\tilde{\kappa}_\Delta$ as

$$\tilde{e}_\Delta(Q^2) = \frac{1}{2}[f_{1+}(Q^2) + f_{1-}(Q^2)\bar{T}_3], \quad (27)$$

$$\tilde{\kappa}_\Delta(Q^2) = \frac{1}{2}[f_{2+}(Q^2) + f_{2-}(Q^2)\bar{T}_3]\frac{M_\Delta}{M_N}, \quad (28)$$

and $\bar{T}_3$ is the isospin-$\frac{3}{2}$ matrix defined as

$$\bar{T}_3 = 3\sum_i T_i^\dagger\tau_3 T_i = \begin{bmatrix} 3 & 0 & 0 & 0 \\ 0 & 1 & 0 & 0 \\ 0 & 0 & -1 & 0 \\ 0 & 0 & 0 & -3 \end{bmatrix}. \quad (29)$$

We can also write $\bar{T}_3$ as $\bar{T}_3 = 2M_T$, where M_T is the diagonal matrix with the Δ isospin projections: $M_T = \mathrm{diag}(+3/2, +1/2, -1/2, -3/2)$ [31]. In the limit $Q^2 = 0$ we use

$$e_\Delta = \frac{1}{2}(1 + \bar{T}_3), \qquad \kappa_\Delta = \frac{1}{2}(\kappa_+ + \kappa_-\bar{T}_3)\frac{M_\Delta}{M_N}. \quad (30)$$

The values of $\kappa_\pm$ were fixed in Ref. [83] by the nucleon magnetic moments.

It is convenient also to define

$$\tilde{g}_\Delta = \tilde{e}_\Delta - \tau\tilde{\kappa}_\Delta, \qquad \tilde{f}_\Delta = \tilde{e}_\Delta + \tilde{\kappa}_\Delta. \quad (31)$$

Similarly as for $\tilde{e}_\Delta$ and $\tilde{\kappa}_\Delta$ we suppress the tilde for $Q^2 = 0$.

As both the initial and final states depend of the diquark polarization with the same polarization index, the product of both polarization vectors factors out in the current (24). Then, since the initial and final state have the same mass (M_Δ) [83,84,92],

$$\Delta^{\alpha\beta} \equiv \sum_\lambda \varepsilon^\alpha_{\lambda P_+}\varepsilon^{\beta*}_{\lambda P_-} \quad (32)$$

becomes

$$\Delta^{\alpha\beta} = -g^{\alpha\beta} - \frac{P_+^\alpha P_-^\beta}{M_\Delta^2} + 2\frac{(P_+ + P_-)^\alpha(P_+ + P_-)^\beta}{4M_\Delta^2 + Q^2}. \quad (33)$$

Using Eq. (8) we can decompose the transition current into the contributions from the different components of the wave function:

$$
\begin{aligned}
J^\mu &= 3\sum_\lambda \bar{\Psi}_\Delta j_I^\mu \Psi_\Delta \\
&= 3N^2 \sum_\lambda \bar{\Psi}_S j_I^\mu \Psi_S \\
&\quad + 3aN^2\left\{\sum_\lambda \bar{\Psi}_{D3} j_I^\mu \Psi_S + \sum_\lambda \bar{\Psi}_S j_I^\mu \Psi_{D3}\right\} \\
&\quad + 3bN^2\left\{\sum_\lambda \bar{\Psi}_{D1} j_I^\mu \Psi_S + \sum_\lambda \bar{\Psi}_S j_I^\mu \Psi_{D1}\right\} \\
&\quad + N^2[\mathcal{O}(a^2) + \mathcal{O}(b^2) + \mathcal{O}(ab)],
\end{aligned} \tag{34}
$$

where the last three terms are corrections from the transitions between the same or different D-states. Those terms can be neglected if the admixture coefficients are small. We can write J^μ in a compact form

$$
J^\mu = N^2 J_S^\mu + aN^2 J_{D3}^\mu + bN^2 J_{D1}^\mu \tag{35}
$$

with explicit forms for the currents J_S^μ, J_{D3}^μ and J_{D1}^μ presented in Appendix B.

From the general form (1) and for the wave functions defined by Eqs. (9), (18), and (19), we can write

$$
G_{E0}(Q^2) = N^2 \tilde{g}_\Delta \mathcal{I}_S, \tag{36}
$$

$$
G_{M1}(Q^2) = N^2 \tilde{f}_\Delta\left[\mathcal{I}_S + \frac{4}{5} a \mathcal{I}_{D3} - \frac{2}{5} b \mathcal{I}_{D1}\right], \tag{37}
$$

$$
G_{E2}(Q^2) = 3(aN^2)\tilde{g}_\Delta \frac{\mathcal{I}_{D3}}{\tau}, \tag{38}
$$

$$
G_{M3}(Q^2) = \tilde{f}_\Delta N^2\left[a\frac{\mathcal{I}_{D3}}{\tau} + 2b\frac{\mathcal{I}_{D1}}{\tau}\right], \tag{39}
$$

where $\mathcal{I}_S$ is the overlap between the initial and final S-states,

$$
\mathcal{I}_S = \int_k \psi_S(P_+, k)\psi_S(P_-, k), \tag{40}
$$

and the other overlap integrals, between the initial S and each of the final D-states, are

$$
\mathcal{I}_{D1} = \int_k b(\tilde{k}_+, \tilde{q}_+)\psi_{D1}(P_+, k)\psi_S(P_-, k), \tag{41}
$$

$$
\mathcal{I}_{D3} = \int_k b(\tilde{k}_+, \tilde{q}_+)\psi_{D3}(P_+, k)\psi_S(P_-, k), \tag{42}
$$

with

$$
b(\tilde{k}_+, \tilde{q}_+) = \frac{3}{2}\frac{(\tilde{k}_+ \cdot \tilde{q}_+)^2}{\tilde{q}_+^2} - \frac{1}{2}\tilde{k}_+^2. \tag{43}
$$

The variable $\tilde{k}_+$ is defined by Eq. (12); the variable $\tilde{q}_+$ is defined the same way (just by replacing k by q). The derivation of the previous expressions is presented in Appendix B.

In Eqs. (36)–(39), we chose to have $N^2 = 1$ in order to reproduce the charge of the Δ (the corrections due to the D-state to D-state transition are of the order of a^2, b^2 and ab, as indicated by Eq. (34)).

The first observation to be made on the results (36)–(39) is that, to first order in a and b, the D-states do not contribute to G_{E0}. The second observation is that the D-states provide the only nonvanishing contributions to the electric quadrupole and magnetic octupole form factors, G_{E2} and G_{M3} (opening the possibility for a satisfactory selection of models for the D-states, otherwise specially difficult due to the overshadowing of their effects in G_{M1} by the dominant S-waves).

The definition of $b(\tilde{k}_+, \tilde{q}_+)$ implies that $b(\tilde{k}_+, \tilde{q}_+) = -\mathbf{k}^2 Y_{20}(\hat{k})$ when $Q^2 = 0$ (see Ref. [4] for details). Since the wave functions are independent of $z = \cos\theta$ in that limit, the angular integration of $b(\tilde{k}_+, \tilde{q}_+)$ vanishes in the limit $Q^2 = 0$, and therefore the D-state overlap integrals vanish also. We stress that this result is model independent, since it is a consequence of the orthogonality between the S-state ($L = 0$) and the D-states ($L = 2$).

Consider now the form factors G_{E2} and G_{M3}. They are proportional to $1/\tau$, which is infinite for $Q^2 = 0$. But, as $\mathcal{I}_{D3}$ or $\mathcal{I}_{D1}$ are themselves proportional to τ, both form factors go to a finite value as τ and $Q^2 \to 0$, ensuring no divergence. The proportionality $\mathcal{I}_{D3}$, $\mathcal{I}_{D1} \sim \tau \sim Q^2$ simply comes from the specific dependence of the scalar wave functions on the quark momentum. The proof of that proportionality is done in Appendix C.

This is how a nonzero contribution from the D-state overlap integrals survives for each form factor, in spite of the orthogonality between S and D-states. This same behavior (overlap integral $\mathcal{I} \sim Q^2$ as $Q^2 \to 0$) was already observed also in the Coulomb quadrupole form factor of the $\gamma N \to \Delta$ reaction [4].

To conclude, the form factors G_{E2} and G_{M3} are a consequence of the D-states alone, and they depend on both the admixture coefficients, a and b, and the particular momentum dependence of the D-wave components of the wave function.

A remark about the predictions for the Δ^0 case can also be made: In our approach $G_{E2}(0) = 0$ and $Q_{\Delta^0} = 0$, because the D-state to D-state transitions were neglected. Once those currents are included we may expect a nonzero, although rather small, contribution to $G_{E2}(0)$.

The formulas obtained for the form factors are considerably simplified in the case $Q^2 = 0$. Since in that limit the integrals associated to transitions to the Δ D-states vanish due to angular momentum, via $b(k_+, q_+) \approx Y_{20}(\hat{k})$, we are left with, setting $N^2 \to 1$

$$
G_{E0}(0) = e_\Delta, \tag{44}
$$

$$
G_{M1}(0) = f_\Delta, \tag{45}
$$

$$
G_{E2}(0) = 3ae_\Delta \mathcal{I}'_{D3}, \tag{46}
$$

$$G_{M3}(0) = f_\Delta[a\mathcal{I}'_{D3} + 2b\mathcal{I}'_{D1}]. \quad (47)$$

(The factor $\mathcal{I}_S = 1$ from the normalization of ψ_S was suppressed.) In these equations

$$\mathcal{I}'_{D3} = \lim_{\tau\to 0}\frac{\mathcal{I}_{D3}(\tau)}{\tau} = \frac{d\mathcal{I}_{D3}}{d\tau}(0),$$
$$\mathcal{I}'_{D1} = \lim_{\tau\to 0}\frac{\mathcal{I}_{D1}(\tau)}{\tau} = \frac{d\mathcal{I}_{D1}}{d\tau}(0),$$

where $\mathcal{I}_{D3}$ and $\mathcal{I}_{D1}$ are defined in Eqs. (41) and (42).

The several moments, corresponding to each of the four multipole form factors, are calculated from Eqs. (7). Note that since the magnetic moment is defined by $G_{M1}(0)$ and $\mathcal{I}_{D1}$ and $\mathcal{I}_{D3}$ vanish at the origin, it follows that the magnetic moment is fixed by the S-state alone.

V. RESULTS

The algebraic results for the form factors given in the previous section were obtained within the covariant spectator formalism, independently of the specific model ingredients. In this section we start to specify the scalar wave functions and the quark current, required for an actual numerical application.

For the quark current we took the parameterization inspired on vector meson dominance (VMD) [4,83,84]:

$$f_{1\pm}(Q^2) = \lambda + \frac{(1-\lambda)}{1+Q^2/m_v^2} + \frac{c_\pm Q^2/M_h^2}{(1+Q^2/M_h^2)^2},$$
$$f_{2\pm}(Q^2) = \kappa_\pm\left\{\frac{d_\pm}{1+Q^2/m_v^2} + \frac{(1-d_\pm)}{1+Q^2/M_h^2}\right\}, \quad (48)$$

where m_v represents a light vector meson $m_v = m_\rho$ (or m_ω), and $M_h = 2M_N$ is the mass of an heavy vector meson which simulates shorter range effects. The parameter λ was adjusted to give the correct quark density number in deep inelastic scattering [83,84], $\lambda = 1.22$. The coefficients c and d were fixed in a previous work to describe the nucleon elastic form factor data. We have $c_+ = 4.16$, $c_- = 1.16$ and $d_+ = d_- = -0.686$ [83]. The particular combination (48) with $c_+ \neq c_-$ gives $f_{1+} \neq f_{1-}$ and therefore breaks isospin symmetry for $Q^2 \neq 0$, essential for a good description of the neutron data. The anomalous magnetic moments $\kappa_+ = 1.639$ and $\kappa_- = 1.823$ generate the nucleon magnetic moment exactly [83]. The parameterization (48) was applied to the nucleon [83,93], Δ electromagnetic form factors [3,82] as well as to the three $\gamma N \to \Delta$ transition form factors [4,84,85,93].

The scalar wave functions depend on the kinematic and dimensionless variable χ, as introduced in Refs. [3,4,83,84,97]:

$$\chi = \frac{(M_\Delta - m_s)^2 - (P-k)^2}{M_\Delta m_s}. \quad (49)$$

We then use [4,93]:

$$\psi_S(P,k) = \frac{N_S}{m_s(\alpha_1+\chi)^3}, \quad (50)$$

$$\psi_{D3}(P,k) = \frac{N_{D3}}{m_s^3(\alpha_2+\chi)^4}, \quad (51)$$

$$\psi_{D1}(P,k) = \frac{N_{D1}}{m_s^3}\left\{\frac{1}{(\alpha_3+\chi)^4} - \frac{\lambda_{D1}}{(\alpha_4+\chi)^4}\right\}. \quad (52)$$

The functions (50)–(52) were chosen for a good description of the $\gamma N \to \Delta$ data [4,84,85]. The coefficient λ_{D1} in ψ_{D1} was determined by imposing the condition that the Δ D1-state and the nucleon S-state are orthogonal [4].

In the applications we consider two different parameterizations for the Δ wave function, both previously derived in the spectator formalism. By comparing the results of two models we can illustrate the sensitivity of the results to model building. The two parameterizations are equivalent with respect to the dominant S-state, but differ substantially in the D-state contributions. In both models the D-states give minor contributions for the quadrupole $\gamma N \to \Delta$ transition form factors, since they are basically dominated by the pion cloud contributions at low Q^2, which can be parameterized by a simple analytical structure [4]. The first model applied here, labeled Spectator 1 (Sp 1), was derived in Ref. [4] (and named model 4 there) to describe the $\gamma N \to \Delta$ transitions in the physical region. The D-states were calibrated by fitting the experimental data. The second parameterization, labeled Spectator 2 (Sp 2), was given in Ref. [85]. Although it has the same structure as Sp 1, it was adjusted to the lattice QCD data [98] for $\gamma N \to \Delta$, in a pion mass region where the pion cloud effects are negligible, and afterwards extended to the physical pion mass point. The results for the physical region are therefore independent of the pion cloud mechanisms. This feature gives the latter model some robustness, making the procedure, in our opinion, more reliable, and indirectly, constrained by QCD as well. In the first model (Sp 1) there is an admixture of 0.88% for the D3-state and a larger admixture of 4.36% for the D1-state. In the Sp 2 model one obtains an admixture of 0.72% for both D3 and D1. These results supply us with the first quantitative idea of the sensitivity of the D-states to the fitting procedure. The D1-state, specially, shows to be strongly sensitive to that procedure.

A. Electric charge form factor

The results for $G_{E0}(Q^2)$ are shown in Fig. 1. The results for Sp 1 and Sp 2 are exactly the same because both models have the same S-state parameterization, and we chose $N = 1$. In the figure, for the Δ^+ case we compare our results with the physical extrapolation of the Δ^+ form factor from quenched lattice QCD data [73,99]. For the other charge cases, in the absence of lattice data one can use exact isospin symmetry, which amounts to take

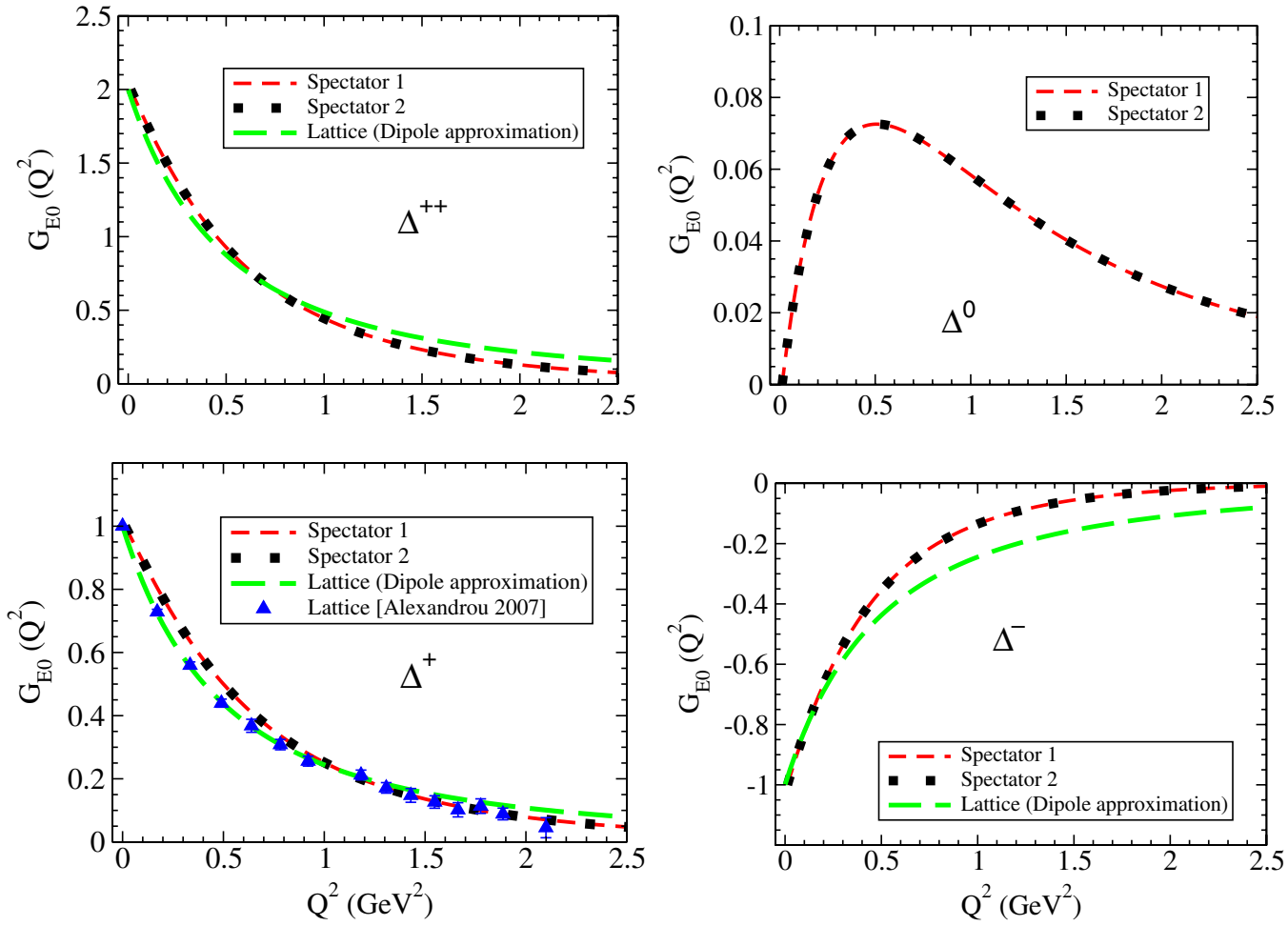

FIG. 1 (color online). G_{E0} form factor. The Lattice data is the physical extrapolation from Refs. [73,99].

$$G_{E0}^{\Delta^{++}}(Q^2) = 2G_{E0}^{\Delta^{+}}(Q^2) = -2G_{E0}^{\Delta^{-}}(Q^2), \qquad (53)$$

where for $G_{E0}^{\Delta^+}$ we used the dipole approximation of the lattice data [73,99]. Although in quenched approximation this symmetry holds, there is no rigorous theoretical justification for it, since breaking of the isospin symmetry can be expected for $Q^2 \neq 0$, and was seen to be consistent with the nucleon data. In fact, the spectator models accommodate isospin asymmetry (through $f_{1+} \neq f_{1-}$ and $f_{2+} \neq f_{2-}$). This is why, in Fig. 2, where $-G_{E0}^{\Delta^-}$ is compared directly with $G_{E0}^{\Delta^+}$, the differences are more significant than what can be observed in Fig. 1 for Δ^+. As expected, the disagreement between $-G_{E0}^{\Delta^-}$ and $G_{E0}^{\Delta^+}$ increases with Q^2. Finally, in Fig. 3 we compare the results for Δ^0 with the neutron electric form factor. Note that the slope near $Q^2 = 0$ is very similar, for both models and G_{En}.

Comparing our calculations with the lattice data (extrapolated to the physical region) from Refs. [73,99] we note, as observed previously in Ref. [3] where only S-states were taken, that both spectator models differ from the lattice data for low Q^2, but are significantly close to the lattice data at larger Q^2. Nevertheless, our models cannot be simulated by a pure dipole dependence as the lattice QCD data can, and one notices that they have a slightly slower falloff with Q^2, implying a smaller charge radius or,

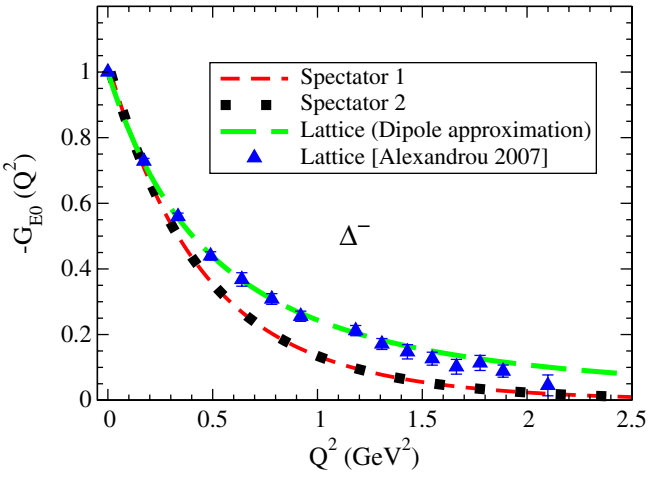

FIG. 2 (color online). Comparing our model results for $-G_{E0}^{\Delta^-}$ with lattice data and the dipole form for $G_{E0}^{\Delta^+}$.

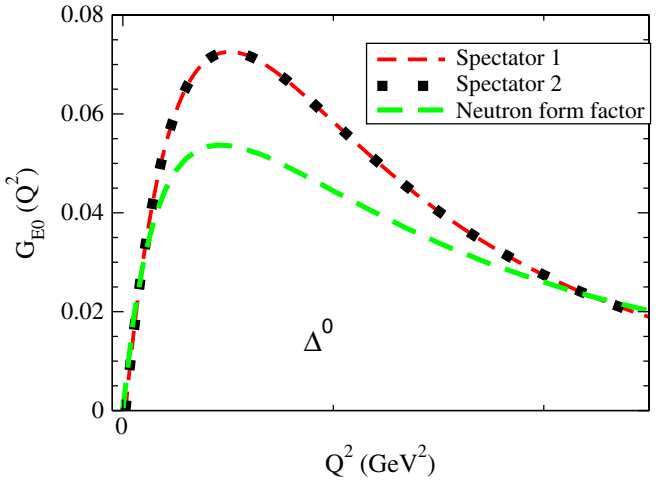

FIG. 3 (color online). Comparing $G_{E0}^{\Delta^0}$ with the neutron form factor.

equivalently, a stronger charge concentration, than suggested by the lattice simulations. In our calculations the squared charge radius of the Δ^+ is 0.29 fm^2 in both models, to be compared with 0.48 fm^2 from the lattice simulation [73,99].

1. Electric charge radius: comparison with other models

The analysis of the charge distribution is naturally done first in terms of the charge radius. For the charged Δ states, the expansion of the charge form factor in powers of Q^2, ($e_\Delta = G_{E0}(0) \neq 0$)

$$G_{E0}(Q^2) = G_{E0}(0)\left[1 - \frac{Q^2}{6}\langle r_{E0}^2\rangle + \mathcal{O}(Q^4)\right], \tag{54}$$

defines the charge squared radius as

$$\langle r_{E0}^2\rangle = -\frac{6}{G_{E0}(0)}\frac{dG_{E0}}{dQ^2}\bigg|_{Q^2=0}. \tag{55}$$

For the case of neutral states (Δ^0), $G_{E0}(0) = 0$, and we use

$$\langle r_{E0}^2\rangle = -6\frac{dG_{E0}}{dQ^2}\bigg|_{Q^2=0}. \tag{56}$$

In some works Eq. (56) [with no normalization to $G_{E0}(0)$ included] instead of Eq. (55), defines the charge radius also for charged particles. The definition (55) has the advantage of being suitable to higher order form factors, namely G_{M1}, without loss of generality. For instance, for the proton, the electric charge and the magnetic dipole form factors have the same dipole dependence on Q^2 at low Q^2, however with no normalization at $Q^2 = 0$ as in Eq. (56), one is led to very different electric charge and magnetic dipole radii. In addition, with Eq. (55) the Δ^- and the Δ^{++} radii can be directly compared with Δ^+. In particular, in a model with exact isospin symmetry [see Eq. (53)] the charge radius is equal for all the charged Δ states if Eq. (55) is used.

The results from our two models, together with a summary of the literature, is presented in Table I. For a better interpretation of the results we write in the first column the prediction of each calculation for the squared charge radius of the proton, when it is available. Our prediction for the Δ^+ radius is 0.29 fm^2. This number is below the value predicted by a variety of models.

The first estimate of the Δ charge radius was based on NRQM and suggested $r_{\Delta^+}^2 \simeq 1.06$ fm^2 [28], implying a larger spatial distribution for the Δ than for the proton ($r_p^2 \simeq 0.77$ fm^2). That effect was traditionally explained as a result of the repulsive hyperfine interaction of the quarks in spin-triplet state, in contrast with the attractive effect in the singlet state [28]. However, there was, at the time of this explanation, no direct experimental evidence of that fact.

The Δ charge radius was also computed within the MIT bag model [54,100]. One should mention for completeness other approaches, as a Skyrme model [53], a quark-soliton model (QSM) [54], a field theory quark model (FT QM) [55], a relativistic quark model (RQM) [56], a constituent quark model (CQM) [68], a general parameterization of QCD combined with large-N_c (GP/Large N_c) [58] a Goldstone boson exchange (GBE) model [43], a chiral soliton model (χQSM) [62] and a chiral perturbation theory model (χPT) [49]. Although the results differ from model to model, they all have in common the feature that the Δ has a larger charge radius than the proton. The exception is the χPT approach from Ref. [49].

The same trend is seen in CQMs . By taking a nonrelativistic CQM with two-body exchanges, Buchmann *et al.* [31] obtains for the Δ^+ electric radius $r_{\Delta^+}^2$ squared,

$$r_{\Delta^+}^2 = r_p^2 - r_n^2, \tag{57}$$

where r_p^2 and r_n^2 are the proton and neutron squared radius. In the same model $r_{\Delta^0}^2 = 0$. Using recent values for the nucleon radii ($r_p^2 = 0.77$ fm^2; $r_n^2 = -0.116$ fm^2) [52] one obtains $r_{\Delta^+}^2 = 0.88$ fm^2, which, in any case, is larger than r_p^2.

The relation (57) was improved by Dillon and Morpurgo using a general parameterization (GP) of QCD [57] with corrections of the order of 10%–20%. Ameliorating upon Ref. [31], Ref. [33] establishes that the contributions of the impulse approximation are dominant to the charge radius, and that the two-body currents associated with the quark-antiquark pairs are only a small correction (≈ 0.03 fm^2). Using an operator method based on a GP [57] and the large-N_c limit, Buchamnn and Lebed [58] related the four Δ charge radii with the neutron and proton radii. Those results and their uncertainty are also shown in Table I. In this case $r_{\Delta^+}^2 \approx r_p^2$. A similar model, as the GBE model [43], predicts however a smaller Δ charge radius ($r_{\Delta^+}^2 \simeq 0.7$ fm^2). Finally, a calculation within χQSM suggests $r_{\Delta^+}^2 \simeq 0.8$ fm^2 [62].

TABLE I. Summary of existing theoretical and lattice results for $\langle r^2_{E0}\rangle$ (fm^2). For the nucleon one has $r^2_p = 0.766$ fm^2 and $r^2_n = -0.116$ fm^2 [52]. The proton electric radius in the Spectator models is $r^2_p = 0.79$ fm^2 (see model II from Ref. [83]).

$\langle r^2_{E0}\rangle$	p	Δ^{++}	Δ^{+}	Δ^{0}	Δ^{-}
NRQM [28]	0.74		1.06		
MIT bag model [54]	0.53	0.62			
Skyrme [53]	0.52	0.55	0.51	−0.068	0.65
QSM [54]	0.75	0.90			
FT QM [55]	0.56	0.70	0.67	0.03	0.71
RQM [56]		0.520	0.523	0	0.523
CQM (imp) [33]		0.735	0.737	0	0.735
CQM [33]		0.766	0.766	0	0.766
GP/Large-N_c [58]	0.792 ± 0.024	0.85 ± 0.09	0.79 ± 0.09	−0.11 ± 0.09	1.02 ± 0.09
GBE [43]	0.564		0.689	0	
χQSM [62]	0.768		0.794		
χQSM SU(3) [62]	0.770		0.815		
χPT [49]			0.328 ± 0.016		
Spectator [3]			0.33		
Spectator 1		0.35	0.29	−0.104	0.50
Spectator 2		0.35	0.29	−0.104	0.50
Lattice:					
Quenched [78]			0.397 ± 0.088		
Quenched [73,99][a]			0.477 ± 0.008		
Quenched Wilson [74,75]			0.425 ± 0.011		
Dynamical Wilson [74,75]			0.373 ± 0.021		
Hybrid [74,75]			0.411 ± 0.028		
Quenched [76]		0.410 ± 0.057	0.410 ± 0.057	0	0.410 ± 0.057

[a]Extrapolation to the physical point.

Interestingly, the most recent estimates of the Δ electric squared radius [31,33,43,58,62] suggest $r^2_\Delta \approx 0.8$ fm^2, slightly larger, but not significantly larger than the experimental result for the proton $r^2_p \simeq 0.77$ fm^2. In general we can say that the several calculations in the literature predict $r^2_{\Delta^+} > r^2_p$.

Our prediction for the Δ^+ radius (0.29 fm^2) is below all the model calculations identified above. In general these last ones also overpredict the lattice calculations values (∼ 0.40 fm^2 and ∼0.48 fm^2 from [73,99]). Only the estimate of χPT [49] is close to these lattice results.

As for the Δ^0 charge radius, it is interesting to note that it is very close to the neutron radius ($r^2_n = -0.116$ fm^2) in our two models. This comes as no surprise, since, as noticed in Fig. 3, G_{E0} and the neutron electric form factor. have almost the same shape for low Q^2. The result is also consistent with partial quenched χPT (PQχPT) [45].

2. Electric charge radius: comparison with the lattice QCD results

Interestingly, our results are comparable in magnitude with the lattice QCD results in Refs. [74–76]. The lattice results shown in Table I correspond to the lowest pion mass m_π taken by each method ($m_\pi \sim 300$, 400 MeV).

It is expected that the lattice results for the charge radius increase as m_π approaches the physical pion mass value, since it is what happens for the proton, where r^2_p diverges as $m_\pi \to 0$. In fact, the Δ^+ lattice data [73–76] follows approximately the behavior of the proton charge radius as parameterized by χPT in Ref. [101]. This is seen in the left panel of Fig. 4. The vertical line shown indicates the inelastic threshold for pion production, defined by $m_\pi = M_\Delta - M_N$. When this inelastic channel is crossed from above we can conjecture the suppression of Δ^+ charge radius below that point, as suggested by the Δ magnetic moment studies within chiral effective field theory [14,74,81]. In the graph we include also the result of χQSM in Ref. [62] at the physical point, $r^2_{\Delta^+} = 0.794$ fm^2, which is close to the proton charge radius.

In the right panel of the Fig. 4 we illustrate that the Δ^+ lattice charge radius results [76], although comparable with the proton charge radius lattice data [102], are slightly larger, for the same lattice QCD conditions (lattice space $a = 0.128$ fm) and approximation (quenched).

Some care must be taken in comparing model results like ours, and lattice QCD results. First, there are several methods to simulate the quark field in lattice, corresponding to different choices for the actions, as the Wilson (quenched or dynamical) [73–75,103,104], Clover [76,102] or hybrid [74,75] actions. The different choices lead to different results. Besides, lattice methods can differ in the calibration needed to make the connection with the

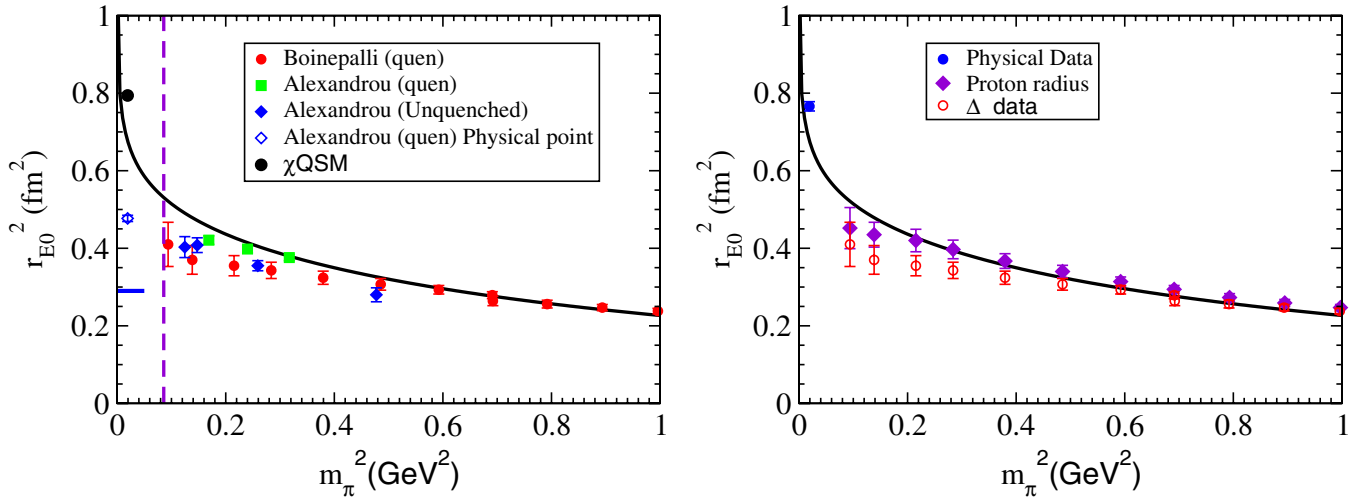

FIG. 4 (color online). Left panel: Δ^+ electric charge radius squared in lattice QCD [76] as a function of the pion mass, compared with the chiral extrapolation (solid line) of the proton charge radius [101]. We show also the result for χQSM [62] and our prediction (horizontal line). The vertical line indicates $m_\pi = M_\Delta - M_N$. Right panel: Δ^+ [76] and proton [102] charge radius in lattice QCD as a function of the pion mass, compared with the chiral extrapolation of the proton charge radius [101] (solid line). The experimental result for r_p^2 [52] is also included.

physical limit. That can be done by adjusting the lattice spacing using the Sommer method [102], or the physical nucleon mass [104]. The two methods lead to very different predictions for the proton charge radius [102,104].

To finish the discussion on the charge radius, we mention that the method from Ref. [45], based on quenched and partial quenched chiral perturbation theory, is useful to extrapolate lattice QCD calculations to the physical limit, and predicts results similar to the ones from our models Sp 1 and Sp 2.

3. Overview of the electric charge form factor

Apart from some deviation at low Q^2, our models give a reasonable description of the lattice data in all their range, when lattice uncertainties are considered.

Our two models (Sp 1 and Sp 2) gives the same result, because there are no D-state contributions for G_{E0} and we have used $N^2 = 1$.

In comparison to other quark models, ours underestimate the charge radius, while it is very close to the lattice data from Refs. [73–75,99]. We predict, as the lattice data does, a stronger charge concentration at the origin for the Δ than for the proton. Still, we obtain a slightly weaker charge concentration than lattice QCD. The quality of the agreement with the quenched lattice data increases for high Q^2, where the meson cloud contribution should be smaller. This supports the idea that at least the valence sector is well described by our covariant spectator model. However, some corrections are expected from the pion cloud at low Q^2, and they are not yet included in our valence quark model. In principle, they will increase the charge radius. Another effect to be added in the future is the inclusion of the D-state to D-state transition. But this effect is expected to be small since it is proportional to the D-state to D-state contributions of the order of a^2, b^2 and ab, with a and b already very small.

B. Magnetic dipole form factor

The magnetic dipole form factor results are shown in Fig. 5, for the four charged Δ states. Only the magnetic moments of Δ^{++} and Δ^+ are experimentally known, and their data points are represented in the graphs for $Q^2 = 0$, according to $\mu_\Delta = G_{M1}(0)\frac{e}{2M_\Delta}$ [5–10]. The extrapolation of the quenched lattice QCD data to the physical point exists only for the Δ^+ case. In that case the dependence on Q^2 of our results is directly compared to that extrapolation. For the other charge cases, in order to compare with the lattice QCD data we use the relation based on exact isospin symmetry

$$G_{M1}^{\Delta^{++}}(Q^2) = 2G_{M1}^{\Delta^+}(Q^2) = -2G_{M1}^{\Delta^-}(Q^2), \qquad (58)$$

together with the dipole approximation for the $G_{M1}^{\Delta^+}(Q^2)$ lattice data. The result extracted from the lattice data [78] using χPT [81] for $Q^2 = 0$ is also shown in the graphs.

Our predictions for Δ^+ are very close to the lattice data. In detail, our results are 7% above the lattice data for low Q^2. However, the lattice errorbars are larger than the ones for the G_{E0} calculation, and our results are close to the limit of the errorbars. For high Q^2 the agreement is very good. In the limit $Q^2 = 0$ our results are consistent with both the experimental points and with the lattice data extrapolation from Refs. [73,81,99]. As found before in the calculation with S-waves only [3], the exception to this good agreement occurs in the Δ^0 case, where [81] predicts a sign

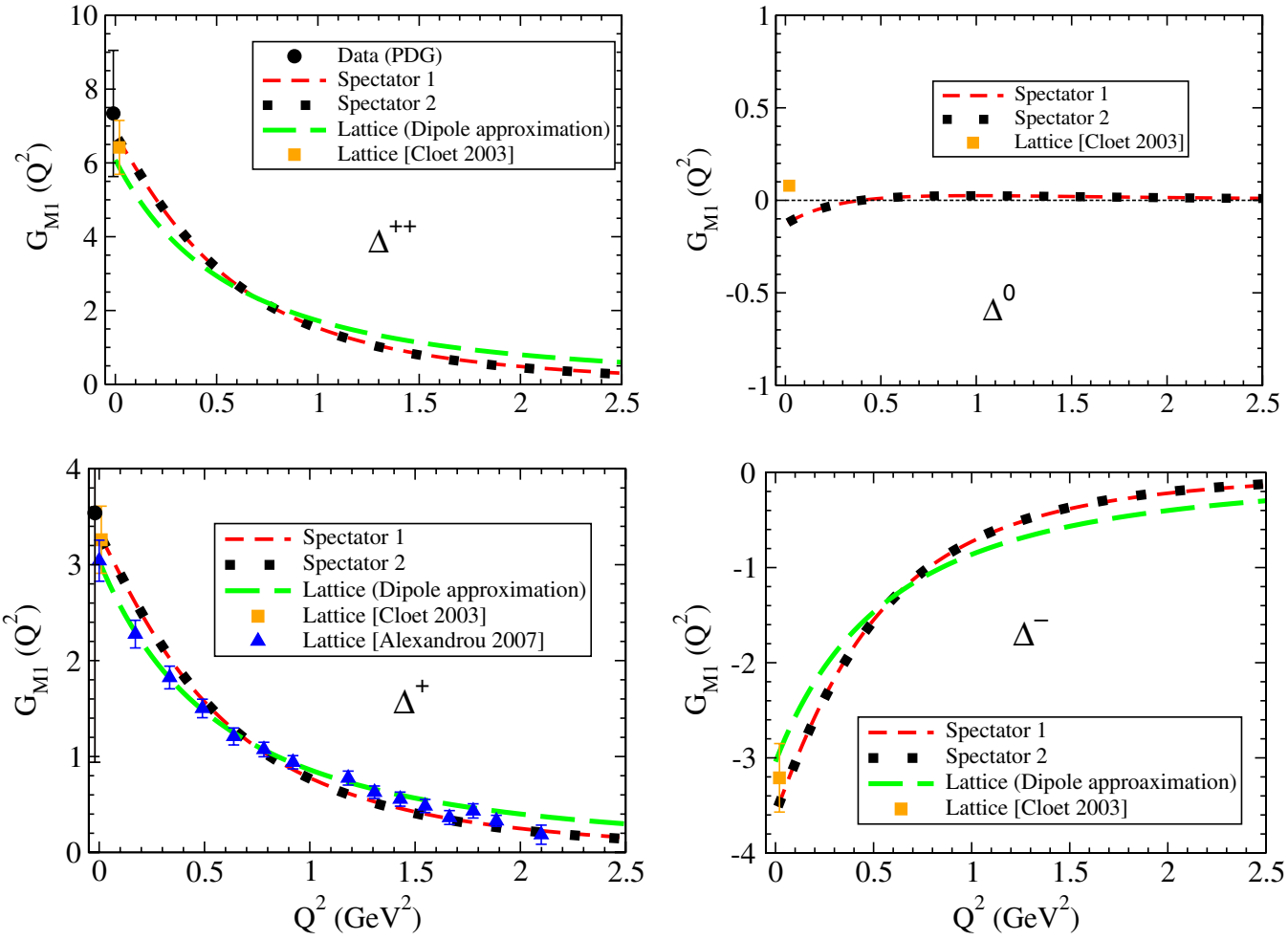

FIG. 5 (color online). G_{M1} form factor. Quenched lattice data from Refs. [73,99]. For Δ^+ we include the experimental result from Ref. [6]: $G_{M1}(0) = 3.54^{+2.37}_{-2.60}(\text{stat} + \text{sys}) \pm 3.94(\text{theor})$ [6]. The theoretical uncertainty for the Δ^+ case is not presented in the figure.

different from ours. This disagreement is not problematic, since in that work the theoretical uncertainty was not explicitly evaluated, and μ_{Δ^0} is expected to be smaller relatively to the charged cases.

In Fig. 6 we compare the effect of the D-states to G_{M1}, for both models Sp 1 and Sp 2. We conclude that the effects of the D-states are small although they increase with Q^2. The small magnitude of these effects is easily understood from Eq. (37) with small admixture coefficients.

1. Magnetic moment: comparison with other models

Our predictions for the magnetic moments are $\mu_{\Delta^{++}} = 5.08\mu_N$ and $\mu_{\Delta^+} = 2.49\mu_N$ for both Sp 1 and Sp 2. The reason why both models lead to exactly the same result is that $G_{M1}(0)$ is determined only by the S-state parameterization, which is the same for the two models. There are some discrepancies between the different experiments, and the Particle Data Group [5] reports the interval of 3.7–7.5 for the Δ^{++} magnetic moment. Our results are in good agreement with that result. Also the result for Δ^+ is consistent if the isospin symmetry is used to estimate the experimental value of μ_{Δ^+}.

The magnetic moment of Δ^+ is traditionally compared with the proton magnetic moment μ_p. In the heavy quark limit (static) approximation they coincide. The SU(6) prediction $G_{M1}(0) = 3.65$ [16] implies that, when expressed in the nucleon magneton units ($\mu_N = \frac{e}{2M_N}$), the Δ^+ and the proton have the same magnetic moment [$\mu_{\Delta^+} = 3.65\frac{e}{2M_\Delta} = 3.65\frac{M_N}{M_\Delta}\frac{e}{2M_N} = 2.79\mu_N$]. Our results for the Δ^+ are $G_{M1}(0) = 3.29$ in both models.

In a previous work [3], we compared our results for $G_{M1}(0)$ without D-waves with several formalisms, namely, relativistic quark models [29], QCD sum rules [32,34], chiral and soliton models [30,41] and dynamical reaction models (DM) based on hadron degrees of freedom [11,14]. Now we compare our calculations, with D-waves included, with a comprehensive update of the more recent results based on χQSM [62], large-N_c [62], SU(2) χPT [47], χPT [49], large N_c-χPT [50], PQχPT [45], GBE [43], QCD sum rules [69], a quark models with sea quark contribu-

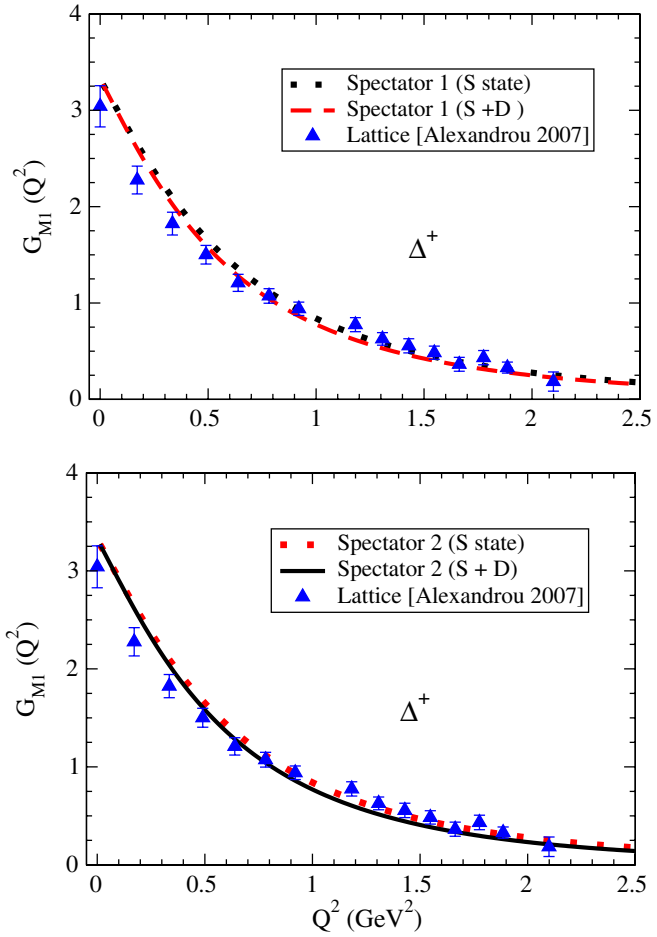

FIG. 6 (color online). Comparing the S-state approach with the effects of the D-states in model Sp 1 and Sp 2. Lattice data from Ref. [73].

tions [40], a hypercentral quark model (HCQM) [48], a gauge/string duality model [44], a recent DM [42] and the U-spin symmetry [46]. For completeness. to this list we add the CQM with one and two-body currents [31]. The predictions for $G_{M1}(0)$ from all these works, together with our own results, are displayed in Table II. The experimental and the SU(6) results are also included. Finally, we present the lattice QCD results [73–76,78,79,81].

In general, all the different models are consistent with the available experimental information.

The PDG interval for $G_{M1}(0)$ corresponds to Δ^{++} and is 4.8–9.8. One has 2.4–4.9 for Δ^+ assuming the isospin symmetry. The symmetric interval hold for Δ^-, in the same approximation. Only Refs. [46,47] for Δ^- are clearly out of the interval.

As for the Δ^0 case, SU(6) and exact isospin symmetry predicts $G_{M1}(0) = 0$, and our models, and in general all models predict contributions an order of magnitude smaller than the magnetic moment of the charged Δ or even zero (excluding the results from DM [42], SU(2) χPT [47] χPT [49] and large N_c-χPT [50]). When μ_{Δ^0} is not zero a negative value is frequently obtained, with a few exceptions. Note that the measurement of μ_{Δ^0} is technically extremely difficult, since on top of the very short Δ lifetime, there is in addition the problem of tracking neutral particles. For all these reasons our knowledge of μ_{Δ^0} will probably be restricted in the near future to values from theoretical models and lattice simulations.

2. Magnetic moment: comparison with the lattice QCD results

Since the lattice simulations of the Δ magnetic moment are performed for heavy quark masses, to compare with phenomenological models the extrapolation to the physical point is needed.

Fortunately, there are nowadays methods based on χPT that can be used for such extrapolations [14,74,81]. The magnetic moment from Ref. [81] is the result of a chiral extrapolation. References [73,79] use a simple functional dependence on the pion mass to extrapolate to the physical point. All the other lattice results in Table II refer to pions masses larger than the physical one.

The dependence of the Δ^+ magnetic moment on the pion mass is presented in Fig. 7 in addition to the result from models Sp 1 and Sp 2 at the physical point. The lattice data in that figure comprises the quenched results from [74–76,78,79], and the unquenched results from [74,75] obtained with the Wilson and hybrid actions [80] using Clover fermions and also the background field method [77,79,80]. The chiral extrapolations of Cloet [81] using the pion loop corrections, and Lee [79] using a simple analytical form, is also on the graph. The inelastic point ($m_\pi < M_\Delta - M_N$) is represented by the vertical line. The solid line in the figure corresponds only to the analytical part of the chiral extrapolation from Cloet *et al.* [81], but the analytical line and the full result lead to similar results for μ_{Δ^+} at the physical point [81] with an accuracy better that 10%. The extrapolation given by Cloet *et al.* compares well with our results.

The main conclusion from the figure is that there are large discrepancies between several lattice calculations. This makes harder to draw conclusions from the comparison of our results with the available lattice data. The unquenched results from Aubin *et al.* [80] for the Δ^+ exceed all the other calculations, including the analytical contribution to the chiral extrapolation [81]. Similarly to Ref. [79], in the Aubin results a significant deviation of the isospin symmetry [see Eq. (58)] is manifest in the Δ^{++} and Δ^+ predictions. Note however that the Aubin results for $\frac{1}{2}\mu_{\Delta^{++}}$, while different from the Δ^+ results, are similar to the results from other calculations. The significant violation of the condition $\frac{1}{2}\mu_{\Delta^{++}} = \mu_{\Delta^+}$, shows that the Aubin calculation violates strongly isospin symmetry, given by Eq. (58).

To understand the discrepancies between the different lattice calculations, it is important to realize that besides

TABLE II. Summary of recent results for $G_{M1}(0)$ compared with the experimental data and the SU(6) result. A compilation of earlier results can be found in Ref. [3]. To obtain μ_Δ in μ_N units (nucleon magneton) use $\mu_\Delta = G_{M1}(0)\frac{M_N}{M_\Delta}\mu_N$.

$G_{M1}(0)$	Δ^{++}	Δ^{+}	Δ^{0}	Δ^{-}
Exp. [5,6]	7.34 ± 2.49	$3.54^{+4.59}_{-4.72}$		
SU(6)	7.31	3.65	0	−3.65
χQSM [62]	6.36	3.09	−0.18	−3.45
Large N_c [62]		3.24		
χPT [49]	7.92 ± 0.17	3.73 ± 0.03	-0.47 ± 0.12	-4.67 ± 0.26
Large N_c-χPT [50]	7.07	3.13	−0.82	−4.77
PQχPT [45]	7.58	3.79	0	−3.79
SU(2) χPT [47]			−0.97	−5.51
GBE [43]	7.34	3.67	0	−3.67
QCDSR [69]	6.34 ± 1.50	3.17 ± 0.75	0	-3.17 ± 0.75
DM [42]	7.16	4.80	−3.29	−4.93
Gauge/string duality [44]	5.81	3.04	0.27	−2.51
$(qqq)q\bar{q}$ model [40]	7.66			
HCQM ($\nu = 0.7$) [48]	5.93	3.00	0.066	−2.95
U-spin [46]				-1.76 ± 0.08
Spectator [3]	6.71	3.29	−0.12	−3.54
Spectator 1	6.66	3.27	−0.12	−3.51
Spectator 2	6.66	3.27	−0.12	−3.51
Lattice:				
Background [79]	6.86 ± 0.24	1.27 ± 0.10	-0.046 ± 0.003	-3.90 ± 0.25
χ-extrapolation [81][a]	6.54 ± 0.73	3.26 ± 0.35	0.079	-3.22 ± 0.35
Quenched (ext) [73,99][a]		3.04 ± 0.21		
Quenched Wilson [74,75]		2.635 ± 0.094		
Dynamical Wilson [74,75]		2.35 ± 0.16		
Hybrid [74,75]		3.05 ± 0.24		
Quenched [76]	5.28 ± 0.92	2.64 ± 0.46	0	-2.64 ± 0.46
Background [76][b]	4.85 ± 0.16	3.15 ± 0.08	0.0013 ± 0.0210	-2.42 ± 0.08

[a]Extrapolation for the physical point. The lattice results from Refs. [74–76,80] include no extrapolation to the physical point. The lattice results correspond, respectively, to $m_\pi = 411$ MeV for quenched Wilson, $m_\pi = 384$ MeV for the dynamical Wilson and $m_\pi = 353$ MeV for the hybrid action [74,75]; $m_\pi = 306$ MeV for quenched from Ref. [76] and $m_\pi = 366$ MeV from Ref. [80].
[b]Ref. [80] uses $\mu_{\Delta^-} = -\frac{1}{2}\mu_{\Delta^{++}}$.

the extrapolation to the physical point, certain lattice calculation of G_{M1} demand an additional extrapolation of Q^2 down to the $Q^2 = 0$ point, given that the minimum lattice momentum Q^2 is nonzero. The most common method uses a given analytical form for the extrapolation. A dipole [73], or an exponential falloff form [74,75] have been used. Another possibility, used by the Adelaide group [76,78,102], applies the scaling between the electric charge form factor and the magnetic dipole form factor, $\frac{G_{M1}(Q^2)}{G_{M1}(0)} = \frac{G_{E0}(Q^2)}{G_{E0}(0)}$. This assumption implies that the magnetic dipole radius squared is the same as the electric charge radius. Note, however that, although the scaling approximation is valid for the proton form factors [83], there is no reason to believe that it holds also for the Δ system.

As a complete different alternative, the background field method [77,79,80] takes the three-quark system interacting at rest ($Q^2 = 0$) with a static magnetic field. Considering the energy shift in the system, which is proportional to the magnetic dipole and also with the magnetic field, the magnetic moment is determined avoiding the uncertainty present in the extrapolation of the form factor method. The different results of [80] may be a consequence of the combination of a strong magnetic field with a not so large lattice volume used in the numeric lattice simulations.

The other problem to consider when comparing between and to different lattice calculations lies in estimating how the quenched approximation deviates from the results from the full QCD calculation, with the same pion mass.

In the SU(6) limit [exact SU(3) flavor symmetry] gives $\mu_{\Delta^+} = \mu_p$. This limit is obtained in quenched QCD when and light and strange quarks have the same mass, i.e. $m_K = m_\pi$, with m_K the kaon mass. In a recent quenched simulation [76] the SU(3) symmetry point corresponds to $m_\pi \simeq 700$ MeV ($m_\pi^2 = 0.485$ GeV^2) [76]. Below this point ($m_\pi < 700$ MeV) $\mu_p > \mu_{\Delta^+}$. This result can be understood analyzing the pion cloud contributions in quenched and in full QCD. As explained in Ref. [76], considering

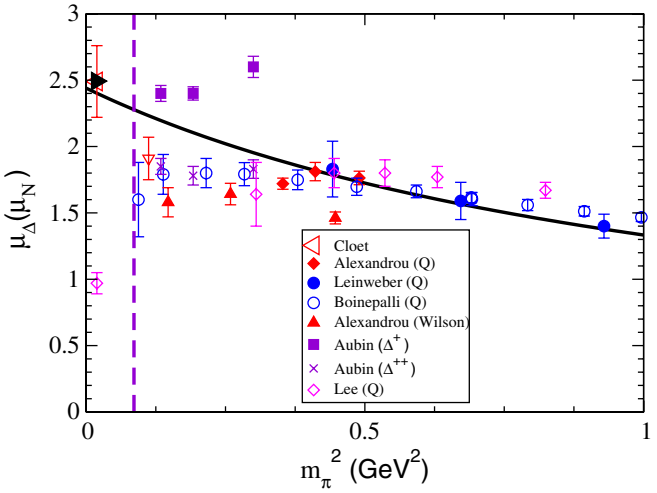

FIG. 7 (color online). Δ^+ magnetic moment from lattice calculations. Quenched lattice data (labeled Q) from [73–75,78,79,99]. Unquenched lattice data from [74,75,80]. The solid line is the analytical contribution for μ_{Δ^+} as derived in Ref. [81]. The result of Sp 1 and Sp 2 (filled $\triangleright$) is also represented.

again Δ^+, for $m_\pi < 700$ MeV, those contributions are negative in quenched approximation while positive in full QCD.

Therefore, for Δ^+ in the region $m_\pi < 700$ MeV, the quenched result underestimates not only full QCD, but even the core contribution, which is already below the full QCD result. This is an artifact of the quenched approximation also observed in Refs. [79,105].

As for μ_{Δ^0}, the extrapolations of Cloet [81] and Lee [79] give different signs. The Aubin result for $m_\pi = 366$ MeV [80] is positive but the error bars are so large that it can also be consistent with zero and negative values. Note that the results of Lee [79] are quenched and the results of Aubin [80] are unquenched.

3. Magnetic dipole radius

We define the magnetic dipole radius squared $\langle r_{M1}^2 \rangle$ by means of the expansion of G_{M1} specified analogously to Eq. (55). The results of the magnetic dipole radius squared are listed on Table III for different models. At low Q^2 they are similar to the ones obtained for the electric charge radius, suggesting a scaling between the electric charge and magnetic dipole form factors, as it was already observed for the proton form factors.

In the comparison between our results and others, the main difference is seen in the Δ^0 magnetic dipole radius, where we obtain a value larger than the radii predicted by all models discussed till this point. This can be just a consequence of the small value of G_{M1} for $Q^2 = 0$. As it happened for the electric radius, the results for the magnetic dipole radius of our two models, as well as the lattice QCD data, underestimate the results obtained with other quark models (see results of Refs. [33,43,62]). This can be a consequence of not including the pion cloud, expected to be important at low Q^2.

TABLE III. Summary of existing theoretical and lattice results for $\langle r_{M1}^2 \rangle$ (fm^2). Ref. [76] the electric and magnetic radius are assumed to be the same. For the nucleon we can consider the result associated with the dipole form $\Lambda^2 = 0.71$ GeV^2.

$\langle r_{M1}^2 \rangle$	r_{Mp}^2	Δ^{++}	Δ^+	Δ^0	Δ^-
MIT bag model [54]	0.38	0.46			
Skyrme [53]		0.47	0.39	−0.16	0.71
QSM [54]	0.61	0.60			
χQSM [62]	0.656		0.634		
χQSM SU(3) [62]	0.665		0.658		
CQM (imp) [33]		0.656	0.656	0	0.656
CQM [33]		0.623	0.623	0	0.623
GBE [43]	0.752		0.689	0	
Spectator [3]			0.37		
Spectator 1		0.32	0.30	1.16	0.36
Spectator 2		0.31	0.30	1.15	0.35
Lattice:					
Quenched [73,99][a]			0.412 ± 0.049		
Quenched Wilson [74,75]			0.240 ± 0.023		
Dynamical Wilson [74,75]			0.230 ± 0.017		
Hybrid [74,75]			0.250 ± 0.033		
Quenched [76]		0.410 ± 0.057	0.410 ± 0.057	0	0.410 ± 0.057

[a]Extrapolation for the physical point. The proton magnetic radius in the Spectator models is $r_{Mp}^2 = 0.74$ fm^2 as extracted from Ref. [83] (model II).

4. Overview of the magnetic dipole form factor

Our results indicate that the S-state contributions are dominant for the Δ magnetic dipole form factors. In the previous section we saw that the same holds for the electric charge form factor. The D-states contribute only with small corrections. In spite of pion cloud effects not being included explicitly here, we predict magnetic dipole distributions similar to the lattice results. When compared with other quark models we predict a larger concentration of the magnetic dipole distribution at the origin.

C. Direct comparison with lattice QCD

We have compared our results for the magnetic dipole form factor with the extrapolation to the physical pion mass point of the quenched lattice QCD data. But quenched data include pion cloud effects only partially, and lattice results based on quenched approximation are known to underestimate the full QCD result, as discussed. Fortunately, the Δ form factors were recently also evaluated with unquenched methods. Those include sea quark effects from up and down quarks (Wilson action), and also from the strange quark (hybrid action) [74,75]. For those calculations there are no extrapolations to the physical pion mass limit available. In these cases we could only compare our models directly to the published lattice data. Figure 8 shows the results for G_{E0} and G_{M1} corresponding to the lowest pion mass in each case: 411 MeV (quenched), 384 MeV (Wilson action) and 353 MeV (hybrid action). In addition to the results of Ref. [75] we include the point corresponding to $m_\pi = 306$ MeV from Ref. [76].

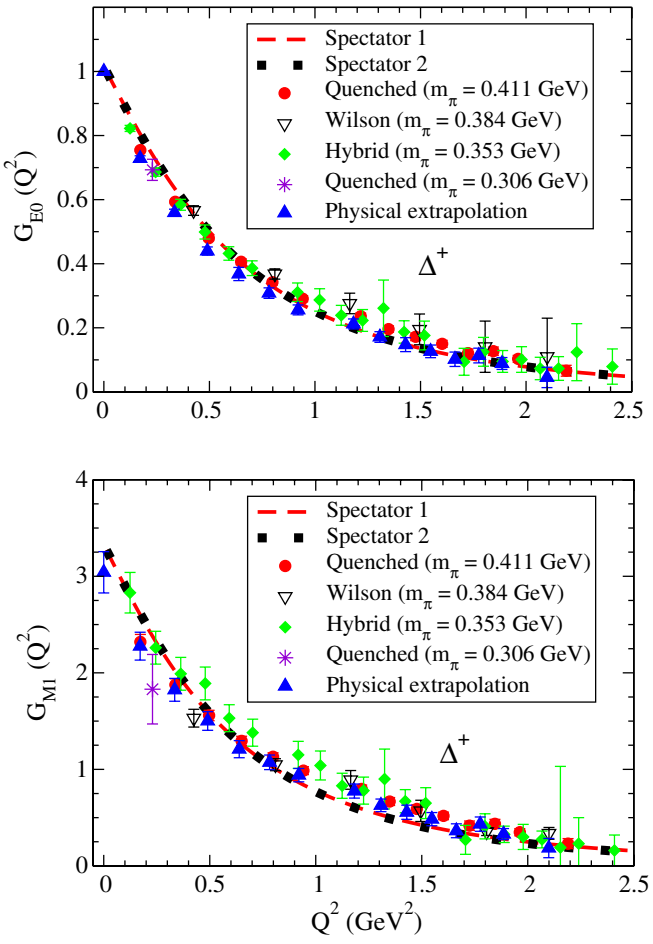

FIG. 8 (color online). Lattice data from Refs. [73,75,76] underestimates the other results.

Surprisingly, our two models also reproduce the magnitude of the lattice QCD data even in the nonphysical pion mass region. The agreement between our predictions for G_{M1} and the lattice data at low Q^2 explains why the $\langle r^2_{M1}\rangle$ values obtained with our models are close to the lattice values, as seen in Table III. Note that although different methods give very similar results for G_{M1} they exceed slightly the physical point (one data point from Ref. [76] is the exception, probably as a consequence of the small pion mass considered).

D. Electric quadrupole form factor

Because of Eqs. (36) and (37), the charge and magnetic dipole form factors are essentially determined by the S-state component of the Δ wave function. But without D-states in the Δ wave function the electric quadrupole form factor is identically zero. As such, G_{E2} measures a transition between the S-state and the D3-state ($\mathcal{S} = 3/2$, $L = 2$) of the Δ [see Eq. (38)]. Differently said, the D3-state induces a deformation in the Δ system that builds up a nonzero electric quadrupole proportional to the D3-state admixture parameter a.

1. Electric quadrupole moment

The electrical quadrupole moment Q_Δ is defined as $Q_\Delta = G_{E2}(0)\frac{e}{M^2_\Delta}$. The shape of the Δ can be interpreted according to the sign of Q_Δ, if one relates in the Breit frame the charge distribution to the form factors in the nonrelativistic limit. For a positive charge, a deformation extended along the equatorial region ($Q_\Delta < 0$) corresponds to an oblate distribution (pancakelike) and a deformation along the polar axis ($Q_\Delta > 0$) to a prolate distribution (cigarlike). Alternative interpretations of deformation can be introduced, and give different insight on the structure [74,75]. More details about this issue of deformation are presented in a separate work [89].

Our results for G_{E2} at $Q^2 = 0$ are shown in Table IV. Since G_{E2} depends only on the state D3, $G_{E2}(0)$ is determined by $\mathcal{I}'_{D3}$ which is -7.00 (Sp 1) or -6.65 (Sp 2). Besides, the D3-state admixture coefficents are not very different (0.88% versus 0.72%) and therefore both models give similar values for $G_{E2}(0)$. In our case, $Q_{\Delta^0} = 0$ because the D-state to D-state contributions were neglected. But nonzero although small contribution for Q_{Δ^0} may appear otherwise.

TABLE IV. Summary of existing theoretical and lattice results for $G_{E2}(0)$. To obtain the electric quadrupole moment use $Q_\Delta = G_{E2}(0)\frac{e}{M_\Delta^2}$ with $M_\Delta = 6.24$ fm^{-1}.

$G_{E2}(0)$	Δ^{++}	Δ^{+}	Δ^{0}	Δ^{-}
NRQM (Isgur) [63,66]	-3.82	-1.91	0	1.91
NRQM [66]	-3.63	-1.79	0	1.79
Skyrme [67]	-3.39	-1.21	0.94	3.12
Buchmann (imp) [31]	-2.49	-1.25	0	1.25
Buchmann (exc) [31]	-9.28	-4.64	0	4.64
χPT [30]	-3.12 ± 1.95	-1.17 ± 0.78	0.47 ± 0.20	2.34 ± 1.17
χPT [49]	-1.05 ± 1.29	-0.94 ± 0.58	-0.86 ± 0.94	0.78 ± 0.78
QMCM [65]	-2.34	-0.81	0.70	2.22
χQSM [62]		-2.15		
QCDSR [69]	-0.0452 ± 0.0113	-0.0226 ± 0.0057	0	0.0226 ± 0.0057
GP(QCD) [51]		-7.02 ± 4.05		
Spectator 1	-4.08	-2.04	0	2.04
Spectator 2	-3.41	-1.71	0	1.71
Lattice:				
Quenched [78]	-0.7 ± 2.8	-0.4 ± 1.4	0	0.4 ± 1.4
Quenched Wilson [75]		-0.81 ± 0.29		
Dynamical Wilson [75]		-0.87 ± 0.67		
Hybrid [75]		$-2.06^{+1.27}_{-2.35}$		

In Table IV we make comparisons to other works, starting with nonrelativistic quark models (NRQM) e.g. the classic Isgur model [63]. In those models the quark D-states are a consequence of the hyperfine interaction in the presence of a confinement mechanism. Then Q_Δ was estimated in terms of the admixture coefficients for the symmetric, antisymmetric and with mixed symmetry components in the S and D-state wave functions, together with a confinement parameter associated to the spherical harmonic oscillator (interpreted as the quark core radius) [28,31], and assuming, as we do here, that the transition between D-states is negligible.

In this type of NRQM description, where the valence quark degrees of freedom and the electromagnetic interaction are reduced to the impulse approximation (which includes only the one-body current), it was possible to relate the Δ charge distribution with the neutron charge distribution [66,106] according to

$$Q_\Delta^{(\mathrm{imp})} = \frac{2}{5} e_\Delta r_n^2, \tag{59}$$

where r_n^2 is the neutron squared radius, and the index (imp) holds for impulse approximation (one-body current). Equation (59) is a parameter free relation, since it is independent of the admixture coefficients and of the confinement parameter. Considering a recent estimate $r_n^2 = -0.116$ fm^2 [52], one has $Q_{\Delta^+} \simeq -0.0464$ fm^2, or $G_{E2}^{\Delta^+}(0) \simeq -1.81$, in close agreement to the result of Ref. [66]. Similar numerical results were obtained by Buchmann *et al.* [31] with a different combination of values for the admixture coefficients together with the confining parameter.

To estimate the nonvalence contribution for Q_Δ absent in the formulas above, Buchmann *et al.* [31] included two-body currents for the quark-antiquark production mechanisms, and obtained

$$Q_\Delta^{(\mathrm{exc})} = e_\Delta r_n^2. \tag{60}$$

In this case no D-state admixture is considered. Although it is a consequence of the constituent quark formalism, this result has again the feature of being parameter independent [31], and could even be obtained in the large N_c limit [60]. Later, Eq. (60) was improved by means of a GP of QCD [51,57,61], for the inclusion of higher order terms. From the $\gamma N \to \Delta$ electric quadrupole data [51] the value $G_{E2}(0) = -7.02 \pm 4.05$ was obtained. Note that this result, and already the result from Eq. (60) [31], are large when compared to the other calculations compiled in Table IV.

The other results in the literature are based on χPT [30,49,72], on a quark-meson coupling model (QMCM) [65], on a Skyrme model [67], and more recently χQSM [62] and QCD sum rules [69]. For completeness we mention as well calculations of PQχPT in the heavy quark mass limit [45,71], and relations between the electric quadrupole moments for different charge Δ states [59,70].

From lattice QCD there are earlier calculations from Leinweber [78], and recent simulations [62,74–76] based on different approaches: quenched, dynamical Wilson (u and d sea quarks) and hybrid action (also s quarks included). The lattice results are also presented in Table IV.

Our model compares well with the NRQM from Refs. [31,63,66] based only on the valence quark degrees of freedom (see Table IV), although it overshoots the QCD sum rules [69]. Mixed descriptions, involving quarks and mesons, in particular, pions, as degrees of freedom as χPT [30,49], QMCM [65] and χQSM [62] suggest that the meson cloud can be important, although not as significant as Eq. (60) seems to imply.

2. Dependence of G_{E2} with Q^2

Before we compare our results with lattice QCD data we investigate the dependence of G_{E2} on Q^2. The results for $G_{E0}(Q^2)$ are presented in Fig. 9, for the models Sp 1 and Sp 2, for all the Δ charge cases. For Δ^+ the results are also compared with the more complete unquenched lattice QCD simulation (hybrid action) for the lightest pion mass available ($m_\pi = 353$ MeV) [75]. As a reference result we include also the χPT calculation from [49] and the NRQM from Eq. (59). [The χPT prediction for Δ^0 is out of the scale although the error bars are consistent with our result (zero)]. The hybrid action considers u and d quarks as valence quarks, and u, d and s as sea quarks. Therefore pion cloud contributions are included, although the results are not extrapolated to the physical pion mass.

In the left panel of Fig. 10 our models for Δ^+ electric quadrupole are compared with other lattice QCD methods, namely, the quenched calculation with $m_\pi = 411$ MeV and the dynamical Wilson action calculation with $m_\pi = 384$ MeV, and again the hybrid action results for $m_\pi = 353$ MeV. All the cases shown correspond to the smallest pion mass values of each method. In the same graph, also the lattice analytical extrapolations for $Q^2 = 0$ assuming an exponential dependence in Q^2 are included [Note the significant error bars].

In the right panel of Fig. 10 we compare Sp 1 and Sp 2 with the dipole approximation of the model χQSM from [62], that provides results for G_{E2} as function of Q^2. Additionally, the figure depicts the results from the analytical approximation of lattice QCD of Refs. [74,75], as well as the NRQM and QCDSR [69] results for $Q^2 = 0$.

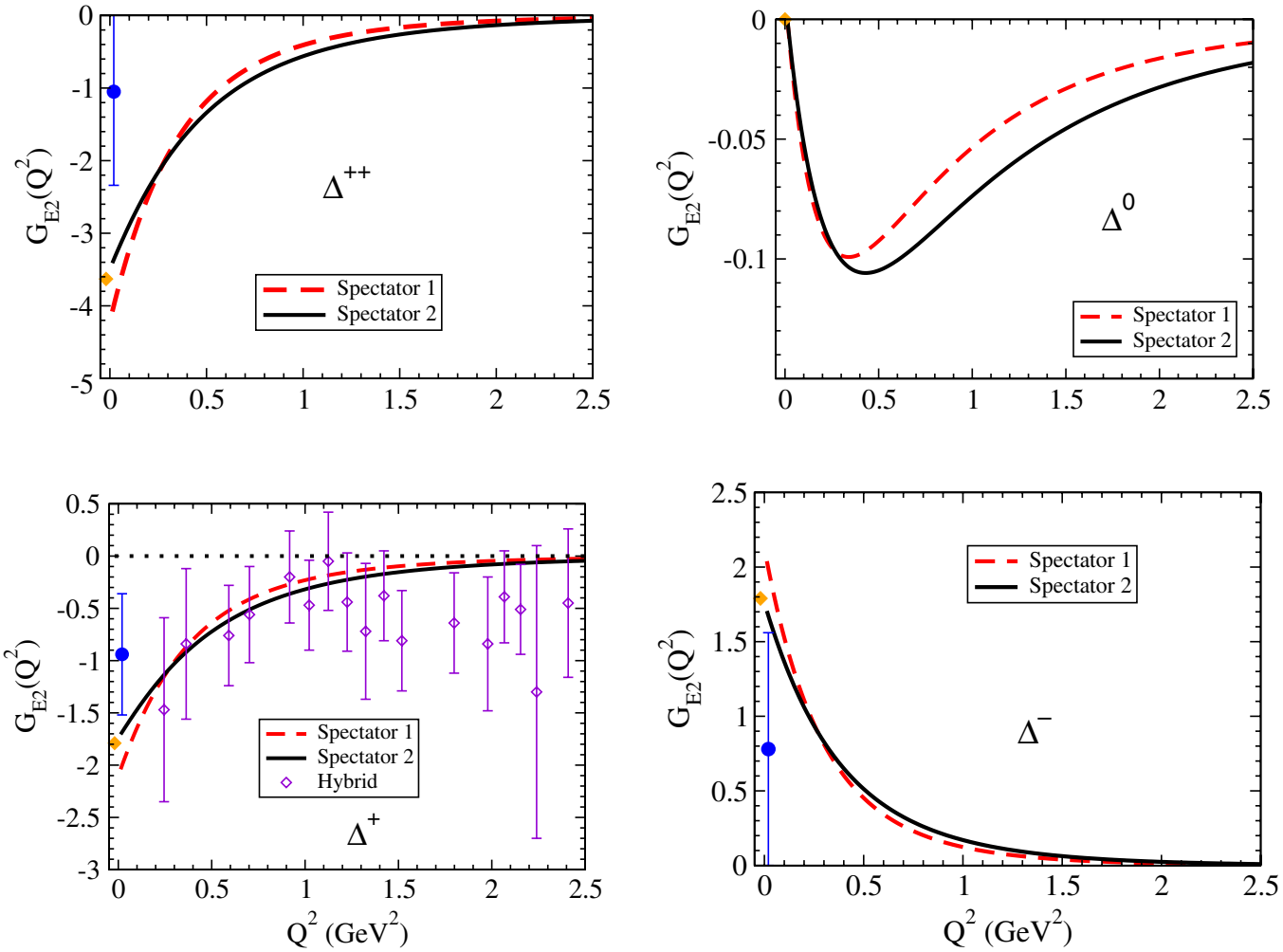

FIG. 9 (color online). Form factor G_{E2}. The Δ^+ lattice QCD points correspond to $m_\pi = 353$ MeV from [75]. The NRQM (◇) is the result of Eq. (59) and (28); χPT (●) is from [49]. The χPT result for Δ^0 is out of the scale (see Table IV).

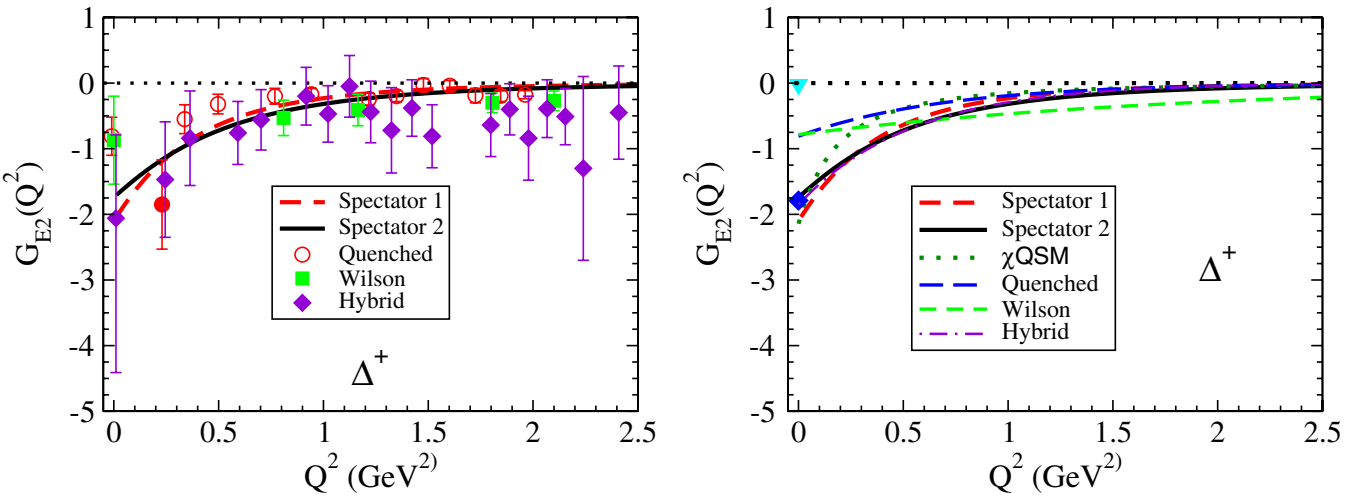

FIG. 10 (color online). Comparing G_{E2} with lattice data from Refs [74,75]. Left panel: quenched data (open ○); Wilson action (filled □) and Hybrid action (filled ◇). The quenched result from [76] for $m_\pi = 306$ MeV is also included (filled ○). Right panel: interpolation of the lattice data [74,75] and χQSM [62]; NRQM (◇) [28] and QCDSR (▽) [69] results are also shown.

From Fig. 10 we conclude that our predictions are close to the hybrid action and the dynamical Wilson action results. Still, our results are larger, in absolute value, than the quenched data, particularly in the low Q^2 region (note that the dynamical hybrid data are consistent with the Wilson and quenched data, within their statistical errors). The difference between our results and different lattice approaches seem to suggest that contrarily to the leading form factors G_{E0} and G_{M1} [3], the meson cloud effect may be important for G_{E2}. Also, the model χQSM, where the contribution of the meson cloud (sea quark contributions) near $Q^2 = 0$ is around 70% [62] falls faster that those models as Q^2 increases. With the exception of Ref. [73] where an extrapolation to the physical point was published, there are no extrapolations of G_{E2} results for the physical point.

In the left panel of Fig. 10 we depict also the lattice data point of Ref. [76] estimated in quenched approximation for $m_\pi = 306$ MeV at $Q^2 = 0.230$ GeV^2. In the limit of the error bars, this point is also consistent with both our models (Sp 1 and Sp 2).

To finish the discussion about $G_{E2}(Q^2)$ we present in Table V the result of our models and the ones from lattice QCD for $\langle r_{E2}^2 \rangle$. Also for this observable Sp 1 and Sp 2 are similar, as we would expect from the graphs from Fig. 9. In both models the radius is in agreement in magnitude with the results from lattice.

TABLE V. Summary of results for $\langle r_{E2}^2 \rangle$ (fm^2).

$\langle r_{E2}^2 \rangle$	Δ^{++}	Δ^+	Δ^0	Δ^-
Spectator 1	0.58	0.53	0.21	0.74
Spectator 2	0.40	0.34	0.18	0.55
Lattice:				
Quenched Wilson [75]		0.336 ± 0.096		
Dynamical Wilson [75]		0.134 ± 0.106		
Hybrid [75]		$0.43^{+1.35}_{-0.20}$		

3. Overview of the electric quadrupole form factor

The Δ electric quadrupole form factor is a measure of the deformation in the charge distribution, and is proportional to the transition coefficient between S and D3-states. Except for the lattice QCD calculations [73–75], and for the model χQSM [62], previous studies of the dependence of the Δ electric quadrupole form factors on Q^2 are almost nonexistent. There are however predictions of several models at the photon point. Our model is consistent with most of these calculations based on valence quark degrees of freedom.

Our results agree also with the dynamical lattice QCD simulations with (Wilson and hybrid actions) for the lightest pion cases. Lattice QCD data seems to suggest that sea quark effects play a more important role for G_{E2} than for G_{E0} and G_{M1}, but the statistics must still be increased to allow more definitive conclusions.

The similarity of the D3-state parameterization in both our models Sp 1 and Sp 2 leads to very close results for the electric quadrupole form factor. We conclude that the quadrupole electric form factor is not suitable to discriminate between our models.

E. Magnetic octupole form factor

The third order form factor, G_{M3}, did not attract as much attention as the first order (G_{E0}, G_{M1}) and the second order (G_{E2}) form factors. Even for the magnetic octupole moment, $\mathcal{O}_\Delta$, there is no experimental information whatsoever, although $\mathcal{O}_\Delta$ was estimated considering the earlier NRQM [28]. Interestingly, though, the lattice QCD simu-

TABLE VI. Summary of existing theoretical results for $G_{M3}(0)$. To obtain the magnetic octupole moment use $\mathcal{O}_\Delta = G_{M3}(0)\frac{e}{2M_\Delta^3}$, with $M_\Delta = 6.24\ \text{fm}^{-1}$.

$G_{M3}(0)$	Δ^{++}	Δ^{+}	Δ^{0}	Δ^{-}
QCDSR [69]	-0.0925 ± 0.0234	-0.0462 ± 0.0117	0	0.0462 ± 0.0117
GP [2]	-11.68	-5.84	0	5.84
χPT [49]	-4.07 ± 9.49	-2.03 ± 4.76	0.059 ± 0.036	2.26 ± 4.52
Spectator 1	-0.049	-0.024	0.000 84	0.026
Spectator 2	-3.51	-1.72	0.064	1.85

lations in Ref. [73] raised the question whether it is possible to determine the sign of $\mathcal{O}_\Delta$ accurately, or equivalently, with respect to the magnetic dipole distribution, whether the Δ is prolate ($\mathcal{O}_\Delta$ positive) or oblate ($\mathcal{O}_\Delta$ negative). The first lattice QCD simulation [78] was not accurate enough to answer this question. The recent work of the MIT-Nicosia group [73] based on the quenched approximation increased the hope that G_{M3} or at least its sign can determined unequivocally by lattice QCD. This was a challenge for both MIT-Nicosia [75] and Adelaide groups [76]. The results from Ref. [76] (which are quenched) suggest a negative sign (i.e. a prolate distribution) for G_{M3}. Nevertheless, one has to check whether the results for G_{M3} are not significantly affected by the sign of the pion loop contributions, as it happens for G_{M1} (see discussion in Sec. V B). One should note that those results correspond to large mass pions, and no physical extrapolation was performed yet.

From the theoretical point of view, the publication of lattice QCD results for G_{M3} triggered the application of quark models to compute $\mathcal{O}_\Delta$ and G_{M3}. Buchmann and Henley [2] using a CQM with pion cloud, two-body currents and the GP formalism [57] predicted $\mathcal{O}_{\Delta^+} = -0.012e\ \text{fm}^3$. The magnetic octupole was also recently predicted by QCD sum rules [69] and χPT [49]. Predictions for $G_{M3}(Q^2)$, based on the χSQM are expected for a near future [62]. χPT predicts a nonzero octupole moment only at two meson loops level [30]. Within PQχPT in the heavy quark mass limit at one meson loop level, one has $G_{M3}(0) = 0$ [45,71], consistently with the quenched QCD data from Ref. [76] for large pion mass values.

A summary of the predictions for $G_{M3}(0)$, including our results from models Sp 1 and Sp 2, is presented in Table VI.

In the covariant spectator quark model, according to Eq. (47), $G_{M3}(0)$ depends only on the integrals $\mathcal{I}'_{D3}$, $\mathcal{I}'_{D1}$ and the admixture coefficients a and b. For model Sp 1 one was $\mathcal{I}'_{D3} = -7.00$, $\mathcal{I}'_{D1} = 1.59$. As for model Sp 2, $\mathcal{I}'_{D3} = -6.65$, $\mathcal{I}'_{D1} = 0.24$. For the model Sp 1 the large contribution of the D1-state (4%) cancels the D3 contribution leading to an almost zero value to $G_{M3}(0)$. This entails a dramatic difference between the results of models Sp 1 and Sp 2, as we can see from Table VI. Model Sp 1 gives negligible contributions for $G_{M3}(0)$. The result from Sp 2 lies between the negligible predictions of QCD sum rules, and the large value of Buchmann [2] based on a pion cloud model and the GP formalism [2,57,60]. For completeness, and following the previous sections, the results for $\langle r^2_{M3}\rangle$ are also presented in Table VII.

The differences between models Sp 1 and Sp 2 for G_{M3} are clear from Fig. 11. For $Q^2 \neq 0$ the cancellation between D1 and D3 contributions in model Sp 1 still exists, although it is not as spectacular as in the $Q^2 = 0$ case. We note also the change of sign in Sp 2 for $Q^2 \approx 0.4\ \text{GeV}^2$. It would be interesting in the future to compare the Q^2 dependence of model Sp 2 with alternative models or with lattice data. The estimates of QCD sum rules [69], χPT [49] and GP [2] for $Q^2 = 0$ are also included in the graphs. For the Δ^+ we show the lattice data of Ref. [76] for the pion mass $m_\pi = 306$ MeV at $Q^2 = 0.230\ \text{GeV}^2$. In the graph we represent also the range of variation obtained in Ref. [73] from calculations with several pion masses.

The results for Δ^+ from model Sp 2 underestimate in absolute value the lattice QCD data point from Ref. [76] for $m_\pi = 306$ MeV, but it is consistent with the central value of χPT [49]. We note, although, that the errorbands are significant. The predictions of Sp 2 are also consistent the data from Ref. [73], within an interval associated with several pion masses. It will be interesting in the future to verify if the quenched approximation affects crucially G_{M3} and if the extrapolation to the physical point introduces significant corrections. To achieve that goal the error bands must be reduced. At that point, Sp 2 can then be better tested.

We can conclude that, contrarily to the form factors analyzed before (electric charge, magnetic dipole and electric quadrupole) the magnetic octupole form factor is extremely sensitive to the D-state parameterization. As for our calculation enabling a decision in favor of Sp 1 or Sp 2, we consider model Sp 2 our best model, because it is better constrained, i.e. it is constrained by not only the experi-

TABLE VII. Summary of results $\langle r^2_{M3}\rangle$ (fm^2).

$\langle r^2_{M3}\rangle$	Δ^{++}	Δ^{+}	Δ^{0}	Δ^{-}
Spectator 1	~150	~150	~150	~150
Spectator 2	1.2	1.1	2.0	1.2

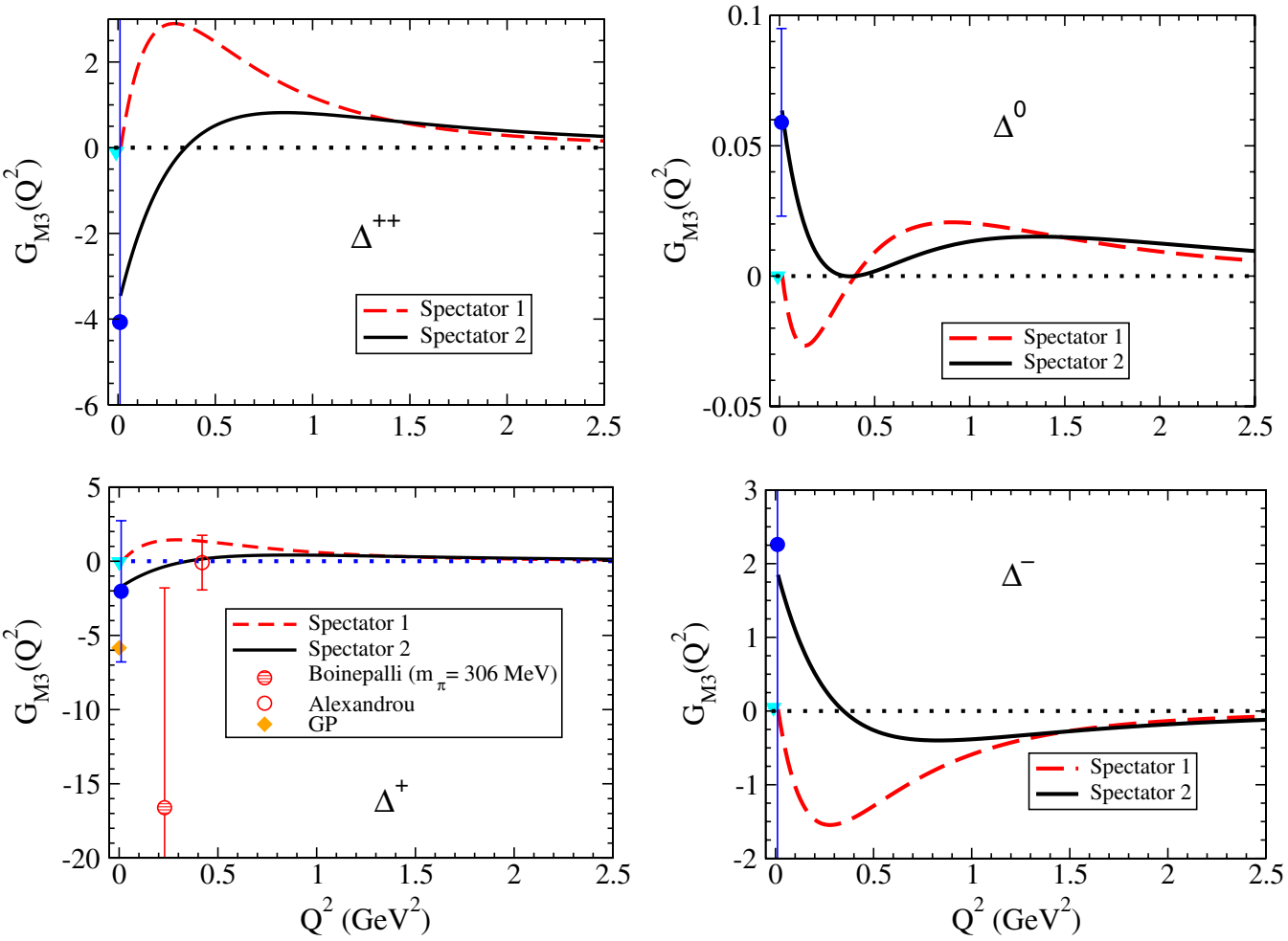

FIG. 11 (color online). G_{M3} form factor. The results for QCDSR (∇) [69] and χPT (filled $\bigcirc$) [49] for $Q^2 = 0$ are shown. Lattice data for Δ^+ from Refs. [73,76] ($m_\pi = 306$ MeV) for $Q^2 = 0.230$ GeV^2, and Alexandrou *et al.* [73] for $Q^2 = 0.42$ GeV^2. The error bar for the data from Alexandrou *et al.* [73] represents the interval of values associated with several pion masses. For Δ^+ the result of GP [2] is also included.

mental but also the lattice data of the reaction $\gamma N \to \Delta$ [85] (see discussion at the beginning of the section). Model Sp 2 predicts a much stronger deformation from the symmetric magnetic dipole distribution. It is also peculiar that the Sp 2 predictions for $G_{M3}(0)$ are similar to the predictions of $G_{E2}(0)$. This implies an almost identical deformation for the electric charge and for the magnetic dipole distribution, if one uses the classical perspective of deformation.

A look at the magnetic octupole charge radius shows also a dramatic difference between the two models. Model Sp 2 predicts typical (although slightly large) values, but model Sp 1 breaks all the scales. That result might however be due to the equation used for $\langle r^2_{M3} \rangle$, which is the analogue of Eq. (55), and breaks down in the limit when $G_{M3}(0)$ gets close to zero. But it might also be a consequence of the pion cloud effects not being explicit in this work.

Overview of the magnetic octupole form factor

Model Sp 2, which is our best model, gives a result for the magnetic octupole closer to the available lattice QCD data. We admit that model Sp 2 is not the last word in the Δ wave function parameterization. Future lattice QCD simulations with increasingly smaller systematic errors may still discard the parameterization of Sp 2 [85]. Note that the quadrupole transition form factors can nowadays be experimentally measured for that reaction (the interaction time in $\gamma N \to \Delta$ is larger than in the reaction $\gamma \Delta \to \Delta$). A direct test of the parameterization will be an even more accurate study of the $\gamma N \to \Delta$ reaction, once more precise data is provided. By using quadrupole form factors (electric and Coulomb) at the physical point [4,84] or, in alternative, their data from lattice QCD [74,85], the valence contributions of the Δ wave function, and, in particular, the small D1- and D3-state contributions, can eventually be

better constrained, to further refine our the predictions for the G_{E2} and G_{M3} Δ form factors.

VI. CONCLUSIONS

In this work we extended the spectator quark model to include the Δ wave function D-states into the matrix elements of the electromagnetic current, in first order in the admixture coefficients of those states. This allowed us to evaluate all the four Δ elastic form factors. We took two models previously calibrated by the two nucleon form factor data [83] and by the form factors for the $\gamma N \to \Delta$ reaction [4,85]. The two models differ in the way they describe the $\gamma N \to \Delta$ quadrupole data. The first model (Sp 1) was derived by fitting the experimental data to the sum of the valence quark contribution with the pion cloud contribution [4]. The second model (Sp 2) was obtained by adjusting only the valence quark contributions to that reaction to the lattice QCD [85], data while still describing the physical data. Because in the last case we fixed the Δ D-state parameters independently of the pion cloud mechanisms, in our view model Sp 2 is more reliable and robust than Sp 1.

Our predictions, based on the valence quark degrees of freedom alone, reproduce well the main features of the lattice results for G_{E0} and G_{M1} when extrapolated to the physical point, except for a some deviation at low Q^2. In particular, the agreement for high Q^2 (say, $Q^2 > 1$ GeV^2) is excellent, indicating that pion cloud effects (not included explicitly in our model) are small for high Q^2 values. This confirms that the valence quarks are the dominant effect in the G_{E0} and G_{M1} form factors, as anticipated in a previous work [3] without the explicit contribution of the D-states. In the low Q^2 region, however, our results for the Δ suggest a smaller charge and magnetic charge radii, when compared with the proton. This can be a limitation caused by the absence of the chiral behavior (or pion cloud effects). Alternatively, it can also represent the real physical case if, as for the Δ magnetic moment, there is a suppression of the charge radius due to the nonanalytical contribution of the inelastic region ($m_\pi < M_\Delta - M_N$). Further lattice QCD studies, preferably unquenched studies, are needed to clarify this point further.

The inclusion of the D-states in the Δ wave function is required to explain the electrical quadrupole and magnetic octupole form factors. The D3-state (spin $3/2$ state with an orbital D-wave) state is needed for a nonvanishing electric quadrupole moment for the Δ. The D1-state (spin $1/2$ with an orbital D-wave), as well as the D3-state (spin $3/2$ with an orbital D-wave), generates nonvanishing contributions for the magnetic octupole form factor. By comparing our results with the available variety of lattice results, we conclude that valence quark contributions are of the same magnitude as the total result. This shows that to establish the magnitude of the contributions of the pion cloud to these observables requires more progress, with more accurate quenched and unquenched lattice data. In its absence for the near future [107], we may estimate the pion cloud effects similarly to what was done for the nucleon and the octet in Ref. [108]. That work concluded that, although significant for the nucleon magnetic moments, pion cloud effects give corrections of less than 8% for the quark anomalous magnetic moments.

Another interesting result to be further explored in the future is that contrary to G_{E2}, G_{M3} is very sensitive to model parameterization. This oversensitivity can be observed in the G_{M3} radius. The value of $G_{M3}(0)$ depends strongly on the D-states admixture and on the overlap between S and D1-states. We obtained an almost complete cancellation of G_{M3} in a particular model (Sp 1). If $G_{M3}(0)$ is in fact very small, then the study of D-state to D-state transitions may became important and should also be explicitly evaluated. Since the direct measurement of a third order multipole is technically difficult, a way out is, in our opinion, the use of the $\gamma N \to \Delta$ (experimental and lattice) data for an even more accurate determination of the D-state admixture following Refs. [4,85], to predict $\mathcal{O}_\Delta$ as done here.

Our best model (Sp 2) gives for Δ^+

$$G_{M1}(0) = 3.27, \qquad G_{E2}(0) = -1.71$$
$$G_{M3}(0) = -1.72. \tag{61}$$

These values correspond to the multipoles:

$$\mu_{\Delta^+} = 2.49\mu_N, \qquad Q_{\Delta^+} = -0.044\ e\text{fm}^2,$$
$$\mathcal{O}_{\Delta^+} = -0.0035\ e\text{fm}^3. \tag{62}$$

As the lattice QCD data for G_{M3} is still affected by a large uncertainty, our results for $\mathcal{O}_{\Delta^+}$ are independent predictions to be tested in the future.

The results (61) and (62), give an oblate deformation for the electric charge and magnetic dipole distributions, considering the *classical* interpretation of deformation. In Ref. [89] we compare this analysis with the one based on transverse density distributions.

The dependence of the G_{M3} form factor on Q^2 that we obtain is very atypical, and it will be interesting if future lattice QCD calculations or alternative hadronic models may confirm our results. It can also happen that forthcoming lattice calculations may require a reparametrization of our model, which would affect in turn our results for the $\gamma N \to \Delta$ (where the quadrupole form factors, electric and Coulomb, are small and sensitive to the D-states.)

In the future, we can extend the model to the lattice QCD regime as suggested in Refs. [85,93,109]. That possibility was already explored in previous applications to the nucleon [93] and $\gamma N \to \Delta$ transition [85,93]. The covariant spectator quark model defines a tool that can be used to extrapolate the lattice results both to the $Q^2 \to 0$ and to the physical pion mass limits. Another strength of this formalism is the possibility of its extension to the strange quark

sector, enabling the application of the model to the octet and decuplet baryon systems. In particular, the application to the Ω^- form factors [109] is very promising, since meson cloud effects (kaon cloud) are expected to be very small in that system. Our predictions could then be compared with lattice simulations nowadays performed at the strange quark physical mass [76,80,110].

ACKNOWLEDGMENTS

G. R. thanks Ross Young, David Richard and Anthony Thomas for helpful discussions. The authors thank also Peter Moron for helpful clarifications relative to Ref. [76] and Constantia Alexandrou for sharing the lattice data from Refs. [73,99]. This work was partially supported by Jefferson Science Associates, LLC under U.S. DOE Contract No. DE-AC05-06OR23177. G. R. was supported by the Portuguese Fundação para a Ciência e Tecnologia (FCT) under Grant No. SFRH/BPD/26886/2006. This work has been supported in part by the European Union (HadronPhysics2 project "Study of strongly interacting matter").

APPENDIX A: GENERIC FORM TO THE CURRENT

Consider the Δ electromagnetic current J^μ

$$J^\mu = \bar{w}_\alpha \Gamma^{\alpha\beta\mu} w_\beta. \tag{A1}$$

The most general form, consistent with parity, G-parity [94], gauge invariance (current conservation) and the properties

$$\begin{aligned} (\not{P}_\pm - M_\Delta) w_\alpha(P_\pm) = 0, \qquad & \bar{w}_\alpha(P_+) P_+^\alpha = 0, \\ P_\pm^\beta w_\beta(P_-) = 0, \qquad & \gamma^\alpha w_\alpha = 0, \end{aligned} \tag{A2}$$

reads

$$\begin{aligned} \Gamma^{\alpha\beta\mu} = {} & (a g^{\alpha\beta} + b q^\alpha q^\beta)\gamma^\mu + (c g^{\alpha\beta} + d q^\alpha q^\beta) P^\mu \\ & + e\left(g^{\alpha\mu} - \frac{q^\alpha q^\mu}{q^2}\right) q^\beta + f\left(g^{\beta\mu} - \frac{q^\beta q^\mu}{q^2}\right) q^\alpha. \end{aligned} \tag{A3}$$

The coefficients a, b, c, d, e and f are general functions of Q^2. Time reversal invariance implies that $\Gamma(P_+, P_-)$ must be symmetric in the permutation $P_+ \rightleftharpoons P_-$ (or $q \to -q$), and then we conclude that

$$f = -e. \tag{A4}$$

Using Eq. (A4), one has

$$\begin{aligned} \Gamma^{\alpha\beta\mu} = {} & (a g^{\alpha\beta} + b q^\alpha q^\beta)\gamma^\mu + (c g^{\alpha\beta} + d q^\alpha q^\beta) P^\mu \\ & + e(g^{\alpha\mu} q^\beta - q^\alpha g^{\beta\mu}). \end{aligned} \tag{A5}$$

To obtain the final form we use the identity due to Fearing [94]:

$$\begin{aligned} g^{\alpha\mu} q^\beta - q^\alpha g^{\beta\mu} = {} & \frac{4M_\Delta^2 + Q^2}{2M_\Delta} g^{\alpha\beta}\gamma^\mu - g^{\alpha\beta}(P_+ + P_-)^\mu \\ & + \frac{q^\alpha q^\beta}{M_\Delta}\gamma^\mu, \end{aligned} \tag{A6}$$

and the Gordon decomposition

$$\frac{(P_+ + P_-)^\mu}{2M_\Delta} = \gamma^\mu - \frac{i\sigma^{\mu\nu} q_\nu}{2M_\Delta}, \tag{A7}$$

which holds between Rarita-Schwinger states and solutions of the Dirac equation. Finally, one has

$$\begin{aligned} \Gamma^{\alpha\beta\mu} = {} & -\left[F_1^* g^{\alpha\beta} + F_3^* \frac{q^\alpha q^\beta}{4M_\Delta^2}\right]\gamma^\mu \\ & - \left[F_2^* g^{\alpha\beta} + F_4^* \frac{q^\alpha q^\beta}{4M_\Delta^2}\right]\frac{i\sigma^{\mu\nu} q_\nu}{2M_\Delta}, \end{aligned} \tag{A8}$$

where F_i^* are linear combinations of a, b, c and e.

APPENDIX B: Δ FORM FACTORS

1. Current J_S^μ

The current J_S^μ was written in Ref. [3] using the Δ S-state wave function of [84]:

$$G_{E0}^S(Q^2) = \tilde{g}_\Delta \mathcal{I}_S, \tag{B1}$$

$$G_{M1}^S(Q^2) = \tilde{f}_\Delta \mathcal{I}_S, \tag{B2}$$

$$G_{E2}^S(Q^2) = G_{M3}^S(Q^2) = 0, \tag{B3}$$

where

$$\mathcal{I}_S = \int_k \psi_S(P_+, k)\psi_S(P_-, k). \tag{B4}$$

As $G_{E2} = G_{M3} \equiv 0$ there is no electric quadrupole neither magnetic octupole originated by the Δ S-states.

2. Current J_{D3}^μ

Consider Eqs. (9) and (19) in a compact notation

$$\Psi_S = -\varepsilon_P^{\alpha *} w_\alpha \psi_S(T \cdot \xi^{1*}), \tag{B5}$$

$$\Psi_{D3} = -3\varepsilon_P^{\alpha *} W_{D3\alpha} \psi_{D3}(T \cdot \xi^{1*}). \tag{B6}$$

The transition between a Δ S and a Δ D3 state can be decomposed in two processes:

(i) S in the initial state (current $J_{S,D3}^\mu$),
(ii) D3 in the initial state (current $J_{D3,S}^\mu$).

In the following we will use the properties of the spin S-states (A2) (S-state) and also

$$\begin{aligned} \not{P}_\pm W_{D3\beta}(P_\pm) = M_\Delta W_{D3\beta}(P_\pm), \qquad & P_\pm^\beta W_{D3\beta}(P_\pm) = 0, \\ \gamma^\beta W_{D3\beta}(P_\pm) = 0. & \end{aligned} \tag{B7}$$

Note that the last identity holds for spin states based in a

spin 3/2 core [4,84]. Simple consequences of those relations are

$$\bar{W}_{D3\alpha}\not{q}w_\beta = \bar{w}_\alpha \not{q} W_{D3\beta} = 0. \tag{B8}$$

Because the S and D3-states have the same core-spin, in general

$$\sum_\lambda \int_k \bar{\Psi}_{D3}(P_+,k)\Psi_S(P_-,k) \neq 0,$$
$$\sum_\lambda \int_k \bar{\Psi}_{S}(P_+,k)\Psi_{D3}(P_-,k) \neq 0,$$

although the result becomes zero for $Q^2 = 0$.

a. Transition $S \to D3$

The transition between an initial Δ S-state (momentum P_-) and a final Δ D3-state (P_+) can be written as

$$J^\mu_{S,D3} = 3\sum_\lambda \int_k \bar{\Psi}_{D3}(P_+,k) j_I^\mu \Psi_S(P_-,k), \tag{B9}$$

where the spin and polarization indices are suppressed for simplicity. We can write (B9) as

$$J^\mu_{S,D3} = 3\int_k \{[\bar{W}_{D3\alpha}A^\mu w_\beta]\psi^+_{D3}\psi^-_S\}\Delta^{\alpha\beta}, \tag{B10}$$

where $\psi^+_{D3} = \psi_{D3}(P_+,k)$, $\psi^-_S = \psi_S(P_-,k)$ and

$$A^\mu = (T\cdot\xi^{1*})^\dagger(3j_I^\mu)(T\cdot\xi^{1*}) = \tilde{e}_\Delta\gamma^\mu + \tilde{\kappa}_\Delta\frac{i\sigma^{\mu\nu}q_\nu}{2M_\Delta}. \tag{B11}$$

In the last equation we use the definitions of $\tilde{e}_\Delta$ and $\tilde{\kappa}_\Delta$ from Eqs. (27) and (28).

Using the Gordon decomposition (A7), we write the current (B10) as

$$J^\mu_{S,D3} = \tilde{f}_\Delta \mathcal{J}^\mu_{S,D3} - \tilde{\kappa}_\Delta\frac{(P_+ + P_-)^\mu}{2M_\Delta}\mathcal{R}_{S,D3}, \tag{B12}$$

where $\tilde{f}_\Delta$ is defined by Eq. (31), and

$$\mathcal{J}^\mu_{S,D3} = 3\int_k \{[\bar{W}_{D3\alpha}\gamma^\mu w_\beta]\psi^+_{D3}\psi^-_S\}\Delta^{\alpha\beta}, \tag{B13}$$

$$\mathcal{R}_{S,D3} = 3\int_k \{[\bar{W}_{D3\alpha}w_\beta]\psi^+_{D3}\psi^-_S\}\Delta^{\alpha\beta}. \tag{B14}$$

The expression for $\Delta^{\alpha\beta}$ is given by Eq. (33).

To reduce the current $J^\mu_{S,D3}$ to a form close to the standard one (1), we work the spin algebra using the properties (A2) and (B7). We also use the covariant result of the integration in the azimuthal variable φ [4]:

$$\int_k \mathcal{D}^{\alpha\beta}\psi^+_{D3}\psi^-_S = R^{\alpha\beta}(q,P_+)\int_k b(\tilde{k}_+,\tilde{q}_+)\psi^+_{D3}\psi^-_S, \tag{B15}$$

where

$$b(\tilde{k}_+,\tilde{q}_+) = \frac{3}{2}\frac{(\tilde{k}_+\cdot\tilde{q}_+)^2}{\tilde{q}_+^2} - \frac{1}{2}\tilde{k}_+^2, \tag{B16}$$

$$R^{\alpha\beta}(q,P_+) = \frac{\tilde{q}_+^\alpha\tilde{q}_+^\beta}{\tilde{q}_+^2} - \frac{1}{3}\tilde{g}_+^{\alpha\beta}. \tag{B17}$$

The variable $\tilde{g}_+$ follows Eq. (13) and $\tilde{q}_+$ comes from Eq. (12) with k replaced by q. In the limit $Q^2 = 0$ (initial and final state in the Δ rest frame) $b(\tilde{k},\tilde{q})$ is reduced to $\tilde{k}^2 Y_{20}(\hat{k})$.

At the end, one has

$$\mathcal{J}^\mu_{S,D3} = \bar{w}_\alpha\Big[\frac{1+2\tau}{1+\tau}\frac{q^\alpha q^\beta}{Q^2}\gamma^\mu + g^{\alpha\beta}\gamma^\mu - \frac{1}{1+\tau}\frac{q^\alpha}{M_\Delta}g^{\beta\mu} + 2\frac{1}{1+\tau}\frac{q^\alpha q^\beta}{Q^2}\frac{P^\mu}{M_\Delta}\Big]w_\beta \times \mathcal{I}^+_{D3}, \tag{B18}$$

$$\mathcal{R}_{S,D3} = \bar{w}_\alpha\Big[\frac{3+2\tau}{1+\tau}\frac{q^\alpha q^\beta}{Q^2} + g^{\alpha\beta}\Big]w_\beta \times \mathcal{I}^+_{D3}. \tag{B19}$$

The common integral is defined by

$$\mathcal{I}^+_{D3} = \int_k b(\tilde{k}_+,\tilde{q}_+)\psi^+_{D3}\psi^-_S. \tag{B20}$$

b. Transition $D3 \to S$

The transition between an initial Δ D3-state (momentum P_-) and a final Δ S-state (P_+) can be written as

$$J^\mu_{D3,S} = 3\sum_\lambda \int_k \bar{\Psi}_S(P_+,k) j_I^\mu \Psi_{D3}(P_-,k). \tag{B21}$$

Once again, we suppress the spin and polarization indices for simplicity. We can write (B21) as

$$J^\mu_{D3,S} = 3\int_k \{[\bar{w}_\alpha A^\mu W_{D3\beta}]\psi^+_S\psi^-_{D3}\}\Delta^{\alpha\beta}, \tag{B22}$$

where $\psi^-_{D3} = \psi_{D3}(P_-,k)$, $\psi^+_S = \psi_S(P_+,k)$. The operator A^μ is given by Eq. (B11).

Using again the Gordon decomposition (A7), we obtain

$$J^\mu_{D3,S} = \tilde{f}_\Delta \mathcal{J}^\mu_{D3,S} - \tilde{\kappa}_\Delta\frac{(P_+ + P_-)^\mu}{2M_\Delta}\mathcal{R}_{D3,S}, \tag{B23}$$

where $\tilde{f}_\Delta$ is defined by Eq. (31), and

$$\mathcal{J}^\mu_{D3,S} = 3\int_k \{[\bar{w}_\alpha\gamma^\mu W_{D3\beta}]\psi^-_{D3}\psi^+_S\}\Delta^{\alpha\beta}, \tag{B24}$$

$$\mathcal{R}_{D3,S} = 3\int_k \{[\bar{w}_\alpha W_{D3\beta}]\psi^+_{D3}\psi^-_S\}\Delta^{\alpha\beta}. \tag{B25}$$

To reduce the current (B23) to a form close to the standard one (1), we work the spin algebra as before. We use again the covariant result of the integration in the azimuthal variable φ from Eq. (B15) with the obvious replacement of $P_+ \to P_-$ (which implies $\tilde{k}_+ \to \tilde{k}_-$, $\tilde{q}_+ \to \tilde{q}_-$ and $\tilde{g}^{\alpha\beta}_+ \to \tilde{g}^{\alpha\beta}_-$). One obtains

$$\mathcal{J}^{\mu}_{D3,S} = \bar{w}_{\alpha}\Big[\frac{1+2\tau}{1+\tau}\frac{q^{\alpha}q^{\beta}}{Q^2}\gamma^{\mu} + g^{\alpha\beta}\gamma^{\mu} + \frac{1}{1+\tau}g^{\alpha\mu}\frac{q^{\beta}}{M_{\Delta}} + 2\frac{1}{1+\tau}\frac{q^{\alpha}q^{\beta}}{Q^2}\frac{P_{+}^{\mu}}{M_{\Delta}}\Big]w_{\beta} \times \mathcal{I}^{-}_{D3}, \quad \text{(B26)}$$

$$\mathcal{R}_{D3,S} = \bar{w}_{\alpha}\Big[\frac{3+2\tau}{1+\tau}\frac{q^{\alpha}q^{\beta}}{Q^2} + g^{\alpha\beta}\Big]w_{\beta} \times \mathcal{I}^{-}_{D3}, \quad \text{(B27)}$$

where

$$\mathcal{I}^{-}_{D3} = \int_k b(\tilde{k}_-, \tilde{q}_-)\psi^{-}_{D3}\psi^{+}_{S}. \quad \text{(B28)}$$

One can prove now that

$$\mathcal{I}^{+}_{D3} = \mathcal{I}^{-}_{D3} \equiv \mathcal{I}_{D3}. \quad \text{(B29)}$$

One starts with the two integrals with explicit arguments written in the Breit frame. Then we conclude that the integrand of $\mathcal{I}^{+}_{D3}$ is a function of z and the integrand of $\mathcal{I}^{-}_{D3}$ is a function of $-z$. Replacing $z \to -z$ we obtain identity in the Breit frame. As the integrals are covariant, the result holds for any frame.

3. Final result

Adding the two currents

$$J^{\mu}_{D3} = J^{\mu}_{S,D3} + J^{\mu}_{D3,S}, \quad \text{(B30)}$$

we define two components (a and b)

$$J^{\mu}_{D3} = J^{\mu}_{a} + J^{\mu}_{b}, \quad \text{(B31)}$$

where

$$J^{\mu}_{a} = \tilde{f}_{\Delta}\mathcal{J}^{\mu}_{D3}, \quad \text{(B32)}$$

$$J^{\mu}_{b} = -\tilde{\kappa}_{\Delta}\mathcal{R}_{D3}\frac{(P_{+}+P_{-})^{\mu}}{2M_{\Delta}}, \quad \text{(B33)}$$

with

$$\mathcal{J}^{\mu}_{D3} = \mathcal{I}_{D3}\Big[\bar{w}_{\alpha}\Big\{2\frac{1+2\tau}{1+\tau}\frac{q^{\alpha}q^{\beta}}{Q^2}\gamma^{\mu} - 2g^{\alpha\beta}\gamma^{\mu} - \frac{1}{1+\tau}\frac{1}{M_{\Delta}}(q^{\alpha}g^{\beta\mu} - q^{\beta}g^{\beta\mu}) + 4\frac{1}{1+\tau}\frac{q^{\alpha}q^{\beta}}{Q^2}\frac{(P_{+}+P_{-})^{\mu}}{2M_{\Delta}}\Big\}w_{\beta}\Big], \quad \text{(B34)}$$

$$\mathcal{R}_{D3} = 2\mathcal{I}_{D3}\Big[\bar{w}_{\alpha}\Big\{\frac{3+2\tau}{1+\tau}\frac{q^{\alpha}q^{\beta}}{Q^2} + g^{\alpha\beta}\Big\}w_{\beta}\Big]. \quad \text{(B35)}$$

Considering the Fearing relation (A6) and the Gordon decomposition (A7) we can finally write

$$\mathcal{J}^{\mu}_{D3} = \frac{2}{1+\tau}\mathcal{I}_{D3} \times \bar{w}_{\alpha}\Big\{\Big[g^{\alpha\beta} + \frac{3}{\tau}\frac{q^{\alpha}q^{\beta}}{4M_{\Delta}^2}\Big]\gamma^{\mu} + \Big[-g^{\alpha\beta} - \frac{2}{\tau}\frac{q^{\alpha}q^{\beta}}{4M_{\Delta}^2}\Big]\frac{i\sigma^{\mu\nu}q_{\nu}}{2M_{\Delta}}\Big\}w_{\beta}. \quad \text{(B36)}$$

From the previous relation and the definition of the form factors F^{*}_{i}, we conclude that the form factors associated with J^{μ}_{a}, from Eq. (B32), are

$$F^{*a}_{1}(Q^2) = -\frac{2}{1+\tau}\tilde{f}_{\Delta}\mathcal{I}_{D3}, \quad \text{(B37)}$$

$$F^{*a}_{2}(Q^2) = \frac{2}{1+\tau}\tilde{f}_{\Delta}\mathcal{I}_{D3}, \quad \text{(B38)}$$

$$F^{*a}_{3}(Q^2) = -\frac{6}{1+\tau}\tilde{f}_{\Delta}\frac{\mathcal{I}_{D3}}{\tau}, \quad \text{(B39)}$$

$$F^{*a}_{4}(Q^2) = \frac{4}{1+\tau}\tilde{f}_{\Delta}\frac{\mathcal{I}_{D3}}{\tau}. \quad \text{(B40)}$$

To evaluate the multipole form factors we consider the transformations (2)–(5). First we note that $F^{*a}_{2} = -F^{*a}_{1}$ and $F^{*a}_{4} = -\frac{3}{2}F^{*a}_{3}$. Then

$$F^{*a}_{1} + F^{*a}_{2} = 0,$$
$$F^{*a}_{1} - \tau F^{*a}_{2} = -2\tilde{f}_{\Delta}\mathcal{I}_{D3},$$
$$F^{*a}_{3} + F^{*a}_{4} = -\frac{2}{1+\tau}\tilde{f}_{\Delta}\frac{\mathcal{I}_{D3}}{\tau},$$
$$F^{*a}_{3} - \tau F^{*a}_{4} = -\frac{2}{1+\tau}(3+2\tau)\tilde{f}_{\Delta}\frac{\mathcal{I}_{D3}}{\tau}.$$

It follows

$$G^{a}_{E0} \equiv 0, \quad \text{(B41)}$$

$$G^{a}_{M1} = \frac{4}{5}\tilde{f}_{\Delta}\mathcal{I}_{D3}, \quad \text{(B42)}$$

$$G^{a}_{E2} = 3\tilde{f}_{\Delta}\frac{\mathcal{I}_{D3}}{\tau}, \quad \text{(B43)}$$

$$G^{a}_{M3} = \tilde{f}_{\Delta}\frac{\mathcal{I}_{D3}}{\tau}. \quad \text{(B44)}$$

Take now the current J^{μ}_{b} from Eq. (B33). Using the Gordon decomposition (A7) and the form of $\mathcal{R}_{D3}$ from Eq. (B35) one concludes that

$$F^{*b}_{1}(Q^2) = 2\kappa_{\Delta}\mathcal{I}_{D3}, \quad \text{(B45)}$$

$$F^{*b}_{2}(Q^2) = -F^{*b}_{1}(Q^2), \quad \text{(B46)}$$

$$F^{*b}_{3}(Q^2) = 2\frac{3+2\tau}{1+\tau}\tilde{\kappa}_{\Delta}\frac{\mathcal{I}_{D3}}{\tau}, \quad \text{(B47)}$$

$$F^{*b}_{4}(Q^2) = -F^{*b}_{3}(Q^2). \quad \text{(B48)}$$

From the previous equations it is easy to conclude that

$$F^{*b}_{1} + F^{*b}_{2} = 0,$$
$$F^{*b}_{3} + F^{*b}_{4} = 0,$$
$$F^{*b}_{1} - \tau F^{*b}_{2} = 2(1+\tau)\tilde{\kappa}_{\Delta}\mathcal{I}_{D3},$$
$$F^{*b}_{3} - \tau F^{*b}_{4} = 2(3+2\tau)\tilde{\kappa}_{\Delta}\mathcal{I}_{D3}.$$

And then,

$$G^b_{E0} \equiv 0, \tag{B49}$$

$$G^b_{M1} \equiv 0, \tag{B50}$$

$$G^b_{E2} = -3(1+\tau)\tilde{\kappa}_\Delta \frac{\mathcal{I}_{D3}}{\tau}, \tag{B51}$$

$$G^b_{M3} \equiv 0. \tag{B52}$$

The magnetic contributions b vanishes for $Q^2 = 0$.

Finally we take the sum of the a and b components. Using the definition for $\tilde{f}_\Delta$, we are left with

$$G^{D3}_{E0}(Q^2) = 0, \tag{B53}$$

$$G^{D3}_{M1}(Q^2) = \tfrac{4}{5}\tilde{f}_\Delta \mathcal{I}_{D3}, \tag{B54}$$

$$G^{D3}_{E2}(Q^2) = 3\tilde{g}_\Delta \frac{\mathcal{I}_{D3}}{\tau}, \tag{B55}$$

$$G^{D3}_{M3}(Q^2) = \tilde{f}_\Delta \frac{\mathcal{I}_{D3}}{\tau}. \tag{B56}$$

Note that the electric form factors include the *electric factor* $\tilde{g}_\Delta$, while the magnetic form factors include the factor $\tilde{f}_\Delta$. To achieve this final form it was essential to include the terms associated with $\mathcal{R}_{D3}$: the result of the overlap between the spin functions associated with core spins $3/2$ (S and D3). Note that, although $\mathcal{I}_{D3}$ vanishes for $Q^2 = 0$, $\frac{\mathcal{I}_{D3}}{\tau} \to$ const as $Q^2 \to 0$.

3. Current J^μ_{D1}

Consider Eqs. (9) and (18) in a compact notation

$$\Psi_S = -\varepsilon^{\alpha *}_P w_\alpha \psi_S(T \cdot \xi^{1*}), \tag{B57}$$

$$\Psi_{D1} = -3\varepsilon^{\alpha *}_P W_{D1\alpha} \psi_{D1}(T \cdot \xi^{1*}). \tag{B58}$$

The transition between a Δ S and a Δ D1 state can be decomposed into two processes:

(i) S in the initial state (current $J^\mu_{S,D1}$),
(ii) D1 in the initial state (current $J^\mu_{D1,S}$).

In the next calculations we use the properties of the spin S-states (A2) (S-state) and D1-state $W_{D1\beta}$:

$$\not{P}_\pm W_{D1\beta}(P_\pm) = M_\Delta W_{D1\beta}(P_\pm), \tag{B59}$$

$$P^\beta_\pm W_{D1\beta}(P_\pm) = 0. \tag{B60}$$

See Ref. [4] for details.

a. Transition $S \to D1$

The transition between an initial Δ S-state (momentum P_-) and a final Δ D1-state (P_+) can be written as

$$J^\mu_{S,D1} = 3\sum_\lambda \int_k \bar{\Psi}_{D1}(P_+, k) j^\mu_I \Psi_S(P_-, k). \tag{B61}$$

We suppress the spin and polarization indicies for simplicity. We can write (B61) as

$$J^\mu_{S,D1} = 3\int_k \{[\bar{W}_{D1\alpha} A^\mu w_\beta]\psi^+_{D1}\psi^-_S\}\Delta^{\alpha\beta}, \tag{B62}$$

where $\psi^+_{D1} = \psi_{D1}(P_+, k)$, $\psi^-_S = \psi_{D1}(P_-, k)$ and A^μ is given by Eq. (B11).

The Gordon decomposition (A7) of the current (B62) gives

$$J^\mu_{S,D1} = 3\tilde{f}_\Delta \int_k \{[\bar{W}_{D1\alpha}\gamma^\mu w_\beta]\psi^+_{D1}\psi^-_S\}\Delta^{\alpha\beta} - 3\tilde{f}_\Delta \mathcal{R}\frac{(P_+ + P_-)^\mu}{2M_\Delta}, \tag{B63}$$

where $\tilde{f}_\Delta$ is defined by Eq. (31), and

$$\mathcal{R} = \int_k \{[\bar{W}_{D1\alpha} w_\beta]\psi^+_{D1}\psi^-_S\}\Delta^{\alpha\beta}. \tag{B64}$$

The orthogonality between the states $W_{D1\alpha}$ and w_β gives

$$\mathcal{R} \equiv 0, \tag{B65}$$

equivalently to

$$3\sum_\lambda \int_k \bar{\Psi}_{D1}(P_+, k)\Psi_S(P_-, k) \equiv 0. \tag{B66}$$

By working the spin algebra and using the covariant integration in the azimuthal variable φ [4]:

$$\int_k \mathcal{D}^{\alpha\beta}\psi^+_{D1}\psi^-_S = R^{\alpha\beta}(q, P_+)\int_k b(\tilde{k}_+, \tilde{q}_+)\psi^+_{D1}\psi^-_S, \tag{B67}$$

with b and R defined, respectively, by (B16) and (B17). At the end, we obtain

$$J^\mu_{S,D1} = \frac{1}{1+\tau}\tilde{f}_\Delta \mathcal{I}^+_{D1}\Big[\bar{w}_\alpha\Big\{\frac{q^\alpha}{M_\Delta}g^{\beta\mu} + 2\frac{q^\alpha q^\beta}{Q^2}\gamma^\mu - 2\frac{q^\alpha q^\beta}{Q^2}\frac{P^\mu_-}{M_\Delta}\Big\}w_\beta\Big], \tag{B68}$$

where

$$\mathcal{I}^+_{D1} = \int_k b(\tilde{k}_+, \tilde{q}_+)\psi^+_{D1}\psi^-_S. \tag{B69}$$

b. Transition $D1 \to S$

We consider now the transition from D1 to S:

$$J^\mu_{D1,S} = 3\sum_\lambda \int_k \bar{\Psi}_S(P_+, k) j^\mu_I \Psi_{D1}(P_-, k). \tag{B70}$$

We conclude that

$$J^{\mu}_{D1,S} = 3\tilde{f}_{\Delta}\sum_{\lambda}\int_k \{[\bar{w}_{\alpha}\gamma^{\mu}W_{D1\beta}]\psi^{-}_{D1}\psi^{+}_{S}\}\Delta^{\alpha\beta}, \quad \text{(B71)}$$

where the orthogonality was used again.

Working through the spin algebra,

$$\int_k \mathcal{D}^{\alpha\beta}\psi^{-}_{D1}\psi^{+}_{S} = R^{\alpha\beta}(q, P_-)\int_k b(\tilde{k}_-, \tilde{q}_-)\psi^{+}_{D1}\psi^{-}_{S}, \quad \text{(B72)}$$

we are left with

$$J^{\mu}_{D1,S} = \frac{1}{1+\tau}\tilde{f}_{\Delta}\mathcal{I}^{-}_{D1}\Big[\bar{w}_{\alpha}\Big\{-g^{\alpha\mu}\frac{q^{\beta}}{M_{\Delta}} + 2\frac{q^{\alpha}q^{\beta}}{Q^2}\gamma^{\mu} - 2\frac{q^{\alpha}q^{\beta}}{Q^2}\frac{P^{\mu}_{+}}{M_{\Delta}}\Big\}w_{\beta}\Big], \quad \text{(B73)}$$

where

$$\mathcal{I}^{-}_{D1} = \int_k b(\tilde{k}_-, \tilde{q}_-)\psi^{-}_{D1}\psi^{+}_{S}. \quad \text{(B74)}$$

Similarly to Appendix B 2, we can prove that

$$\mathcal{I}^{+}_{D1} = \mathcal{I}^{-}_{D1} \equiv \mathcal{I}_{D1}. \quad \text{(B75)}$$

c. Final result

Adding the two currents (B68) and (B73)

$$J^{\mu}_{D1} = J^{\mu}_{S,D1} + J^{\mu}_{D1,S}, \quad \text{(B76)}$$

we obtain

$$J^{\mu}_{D1} = \tilde{f}_{\Delta}\frac{1}{1+\tau}\mathcal{I}_{D1}\bar{w}_{\alpha}\Big\{\frac{1}{M_{\Delta}}(q^{\alpha}g^{\alpha\mu} - q^{\beta}g^{\alpha\mu}) + 4\frac{q^{\alpha}q^{\beta}}{Q^2}\gamma^{\mu} - 4\frac{q^{\alpha}q^{\beta}}{Q^2}\frac{(P_+ + P_-)^{\mu}}{2M_{\Delta}}\Big\}w_{\beta}. \quad \text{(B77)}$$

Using the Fearing-Nozawa relation (A6) and the Gordon decomposition (A7), we are left with

$$J^{\mu}_{D1} = 2\tilde{f}_{\Delta}\frac{1}{1+\tau}\mathcal{I}_{D1}\times\bar{w}_{\alpha}\Big\{\Big[\tau g^{\alpha\beta} + 2\frac{q^{\alpha}q^{\beta}}{4M^2_{\Delta}}\Big]\gamma^{\mu} + \Big[g^{\alpha\beta} + \frac{2}{\tau}\frac{q^{\alpha}q^{\beta}}{4M^2_{\Delta}}\Big]\frac{i\sigma^{\mu\nu}q_{\nu}}{2M_{\Delta}}\Big\}w_{\beta}. \quad \text{(B78)}$$

Comparing the previous equation with Eq. (24), we conclude that

$$F^{*}_1 = -\frac{2}{1+\tau}\tilde{f}_{\Delta}\mathcal{I}_{D1}\tau, \quad \text{(B79)}$$

$$F^{*}_2 = -\frac{2}{1+\tau}\tilde{f}_{\Delta}\mathcal{I}_{D1}, \quad \text{(B80)}$$

$$F^{*}_3 = -2\frac{2}{1+\tau}\tilde{f}_{\Delta}\mathcal{I}_{D1}, \quad \text{(B81)}$$

$$F^{*}_4 = -2\frac{2}{1+\tau}\tilde{f}_{\Delta}\frac{\mathcal{I}_{D1}}{\tau}. \quad \text{(B82)}$$

Note that, although F^{*}_4 includes a factor $1/\tau = 4M^2_{\Delta}/Q^2$, it is not singular. By definition of $b(\tilde{q}, \tilde{k})$ the integral $\mathcal{I}_{D1}$ vanishes as $Q^2 \to 0$ canceling the divergence in $1/\tau$. The condition $\mathcal{I}_{D1} = 0$ when $Q^2 = 0$ is the result of the orthogonality between the states $L = 0$ and $L = 2$.

Using the simple relations

$$F^{*}_1(Q^2) = \tau F^{*}_2(Q^2), \quad \text{(B83)}$$

$$F^{*}_3(Q^2) = \tau F^{*}_4(Q^2), \quad \text{(B84)}$$

we can write

$$F^{*}_1(Q^2) + F^{*}_2(Q^2) = -2\tilde{f}_{\Delta}\mathcal{I}_{D1},$$
$$F^{*}_1(Q^2) - \tau F^{*}_2(Q^2) = 0,$$
$$F^{*}_3(Q^2) + F^{*}_4(Q^2) = -4\tilde{f}_{\Delta}\frac{\mathcal{I}_{D1}}{\tau},$$
$$F^{*}_3(Q^2) - \tau F^{*}_4(Q^2) = 0.$$

Finally,

$$G^{D1}_{E0}(Q^2) \equiv 0, \quad \text{(B85)}$$

$$G^{D1}_{M1}(Q^2) = -\frac{2}{5}\tilde{f}_{\Delta}\mathcal{I}_{D1}, \quad \text{(B86)}$$

$$G^{D1}_{E2}(Q^2) \equiv 0, \quad \text{(B87)}$$

$$G^{D1}_{M3}(Q^2) = 2\tilde{f}_{\Delta}\frac{\mathcal{I}_{D1}}{\tau}. \quad \text{(B88)}$$

In the limit $Q^2 = 0$ only G_{M3} is different from zero.

4. All contributions

Each of the four Δ form factors G_{α} ($\alpha = E0, M1, E2, M3$) is then the result of the three contributions calculated above:

$$G_{\alpha}(Q^2) = N^2[G^{S}_{\alpha}(Q^2) + aG^{D3}_{\alpha}(Q^2) + bG^{D1}_{\alpha}(Q^2)]. \quad \text{(B89)}$$

The final result becomes

$$G_{E0}(Q^2) = N^2\tilde{g}_{\Delta}\mathcal{I}_{S},$$
$$G_{M1}(Q^2) = N^2\tilde{f}_{\Delta}\mathcal{I}_{S} + \frac{4}{5}(aN^2)\tilde{f}_{\Delta}\mathcal{I}_{D3} - \frac{2}{5}(bN^2)\tilde{f}_{\Delta}\mathcal{I}_{D1},$$
$$G_{E2}(Q^2) = 3(aN^2)\tilde{g}_{\Delta}\frac{\mathcal{I}_{D3}}{\tau},$$
$$G_{M3}(Q^2) = \tilde{f}_{\Delta}N^2\Big[a\frac{\mathcal{I}_{D3}}{\tau} + 2b\frac{\mathcal{I}_{D1}}{\tau}\Big]. \quad \text{(B90)}$$

APPENDIX C: PROOF THAT $\mathcal{I}_D \sim Q^2$

Consider the overlap integral

$$\mathcal{I}_D = \int_k b(\tilde{k}_+, \tilde{q}_+)\psi_D(P_+, k)\psi_S(P_-, k), \tag{C1}$$

where D represents an arbitrary (D3 or D1) D-state. The functions ψ_D and ψ_S are, respectively, the D-state and the S-state scalar wave functions written in terms of the dimensionless variable χ, as defined in Eq. (49). That is the only assumption made in this appendix. The function $b(\tilde{k}_+, \tilde{q}_+)$ is defined by Eq. (43).

Although the integral $\mathcal{I}_D$ is covariant the analysis can be considerably simplified in a particular frame. We consider then the rest frame of the final baryon (mass M):

$$P_+ = (M, 0, 0, 0), \qquad P_- = (E, 0, 0, -|\mathbf{q}|), \qquad q = (\omega, 0, 0, |\mathbf{q}|), \tag{C2}$$

where

$$E = \sqrt{M^2 + |\mathbf{q}|^2} = \frac{2M^2 + Q^2}{2M}, \qquad |\mathbf{q}| = \frac{\sqrt{(4M^2 + Q^2)Q^2}}{2M} = \frac{EQ}{M}, \qquad \omega = \frac{P_+ \cdot q}{M} = -\frac{Q^2}{2M}. \tag{C3}$$

In this frame we can write $\tilde{k}_+ = (0, k_x, k_y, k_z)$ and $\tilde{q}_+ = (0, 0, 0, |\mathbf{q}|)$. In the final baryon rest frame $\tilde{k}_+$ and $\tilde{q}_+$ has only spacial components.

It is now trivial to conclude ($\tilde{k}_+ \cdot \tilde{q}_+ = -|\mathbf{q}|k_z$) that

$$b(\tilde{k}_+, \tilde{q}_+) = -\frac{1}{2}(3k_z^2 - \mathbf{k}^2) = -\mathbf{k}^2 Y_{20}(z), \tag{C4}$$

where we used $k_z = |\mathbf{k}|z$, with $z = \cos\theta$. In the final baryon rest frame there is no Q^2 dependence in b, and only the scalar wave functions depend on Q^2.

The momentum dependence of the scalar wave appears through the functions $P_\pm \cdot k$, which become in the final baryon rest frame

$$P_+ \cdot k = ME_s, \tag{C5}$$

$$P_- \cdot k = EE_s + |\mathbf{q}|k_z = EE_s + \frac{EQ}{M}\,\mathrm{k}z. \tag{C6}$$

In the last equation we used $\mathrm{k} = |\mathbf{k}|$. The previous equations show that the angular dependence appears only in the S-state wave function. To perform the angular integration (variable z) for $\mathcal{I}_D$ we need only to consider the factor

$$I = \int dz Y_{20}(z)\psi_S(P_-, k), \tag{C7}$$

where it is implicit that the integration is in the interval $[-1, 1]$.

To proceed, we need to use the momentum dependence of ψ_S. By taking the generic form

$$\psi_S(P_-, k) = \frac{N_S}{D^n}, \tag{C8}$$

where n is a integer ($n \geq 2$), N_S is some normalization constant, and

$$D = \alpha + 2\frac{P_- \cdot k}{Mm_s} - 2 = \beta + 2\frac{EQ}{M^2}\,\mathrm{k}z, \tag{C9}$$

where $\beta = (\alpha - 2) + 2\frac{EE_s}{Mm_s}$.

Factorizing D according with

$$D = \beta\left[1 + 2\frac{EQ}{M^2}\frac{\mathrm{k}}{\beta}z\right], \tag{C10}$$

we can write

$$\frac{1}{D^n} = \frac{1}{\beta^n} \times \left[a_0 + a_1\left(\frac{EQ}{M^2}\frac{\mathrm{k}}{\beta}\right)z + a_2\left(\frac{EQ}{M^2}\frac{\mathrm{k}}{\beta}\right)^2 z^2 + \ldots\right], \tag{C11}$$

where

$$a_j = 2^j\binom{-n}{j} = 2^j\frac{(-n)(-n-1)\ldots(-n-j+1)}{j(j-1)\ldots 1}, \tag{C12}$$

with $j = 0, 1, \ldots$. For $n = 3$, for example, $a_0 = 1$, $a_1 = -6$, $a_2 = 24$, etc.

The angular integration (C7) is now considerably simplified

$$\int dz\left\{Y_{20}(z)\left[a_0 + a_1\left(\frac{EQ}{M^2}\frac{\mathrm{k}}{\beta}\right)z + a_2\left(\frac{EQ}{M^2}\frac{\mathrm{k}}{\beta}\right)^2 z^2 + \ldots\right]\right\} = a_2\left(\frac{EQ}{M^2}\right)^2\left[\int dz z^2 Y_{20}(z)\right] + \mathcal{O}(E^4Q^4), \tag{C13}$$

where the integral of the first term is zero [$\int Y_{20}(z) = 0$], the second term vanishes because is the integral of an odd function (in a symmetric interval), and the same argument holds for the forth them (coefficient a_3). The next nonzero contribution appears only with the fifth term (coefficient a_4). As $\int dz\{z^2 Y_{20}(z)\} = \frac{4}{15}$, the previous result can be written as

$$I = \frac{4}{15}\frac{a_2}{\beta^n}\left(\frac{E}{M^2}\frac{\mathrm{k}}{\beta}\right)^2 Q^2 + \mathcal{O}(E^4Q^4). \tag{C14}$$

We still have to perform the integration in k. However, because $\frac{\mathrm{k}}{\beta} \simeq \frac{1}{2}\frac{M}{E}m_s = \text{const}$ as $\mathrm{k} \to \infty$, all integrals are well defined providing that the original integral is well defined. This means that integration in k preserves the decomposition presented above.

For small Q^2 we need only to consider the leading dependence in Q^2 of each term. Using $\beta_0 = (\alpha - 2) + 2\frac{E_s}{m_s}$, one has

$$I = \frac{4}{15}\frac{a_2}{\beta_0^n}\left(\frac{\mathrm{k}}{M\beta_0}\right)^2 Q^2 + \mathcal{O}(Q^4) \sim Q^2. \quad \text{(C15)}$$

Therefore

$$\mathcal{I}_D \sim Q^2, \quad \text{(C16)}$$

which finishes the proof.

Note that this derivation is independent of n. The only constraint to be imposed is that the power in ψ_S is sufficient to assure the convergence of the integral (in k). An alternative derivation is possible in a different frame, using also the properties of ψ_D. For instance, in the initial baryon rest frame all angular dependence is in ψ_D. Considering ψ_D with the same form of ψ_S from Eq. (C8), we obtain the same limit for small Q^2 using the procedure described before, as it should be.

[1] C. F. Perdrisat, V. Punjabi, and M. Vanderhaeghen, Prog. Part. Nucl. Phys. **59**, 694 (2007).
[2] A. J. Buchmann and E. M. Henley, Eur. Phys. J. A **35**, 267 (2008).
[3] G. Ramalho and M. T. Peña, J. Phys. G **36**, 085004 (2009).
[4] G. Ramalho, M. T. Peña, and F. Gross, Phys. Rev. D **78**, 114017 (2008).
[5] W. M. Yao *et al.* (Particle Data Group), J. Phys. G **33**, 1 (2006).
[6] M. Kotulla *et al.*, Phys. Rev. Lett. **89**, 272001 (2002).
[7] G. Lopez Castro and A. Mariano, Nucl. Phys. **A697**, 440 (2002).
[8] A. Bosshard *et al.*, Phys. Rev. D **44**, 1962 (1991); C. A. Meyer *et al.*, Phys. Rev. D **38**, 754 (1988).
[9] B. M. K. Nefkens *et al.*, Phys. Rev. D **18**, 3911 (1978).
[10] L. Heller, S. Kumano, J. C. Martinez, and E. J. Moniz, Phys. Rev. C **35**, 718 (1987); D. H. Lin, M. K. Liou, and Z. M. Ding, Phys. Rev. C **44**, 1819 (1991); P. Pascual and R. Tarrach, Nucl. Phys. **B134**, 133 (1978);
[11] W. T. Chiang, M. Vanderhaeghen, S. N. Yang, and D. Drechsel, Phys. Rev. C **71**, 015204 (2005); D. Drechsel and M. Vanderhaeghen, Phys. Rev. C **64**, 065202 (2001).
[12] M. Kotulla, AIP Conf. Proc. **904**, 203 (2007).
[13] A. I. Machavariani, A. Faessler, and A. J. Buchmann, Nucl. Phys. **A646**, 231 (1999); **A686**, 601(E) (2001).
[14] V. Pascalutsa and M. Vanderhaeghen, Phys. Rev. Lett. **94**, 102003 (2005).
[15] K. Hikasa *et al.* (Particle Data Group), Phys. Rev. D **45**, S1 (1992) (see p. 482); **46**, 5210(E) (1992).
[16] M. A. B. Beg, B. W. Lee, and A. Pais, Phys. Rev. Lett. **13**, 514 (1964).
[17] Y. A. Chao and R. K. P. Zia, Nuovo Cimento A **19**, 651 (1974).
[18] J. H. Kim, C. H. Lee, and H. K. Lee, Nucl. Phys. **A501**, 835 (1989).
[19] G. Dillon and G. Morpurgo, Z. Phys. C **62**, 31 (1994).
[20] E. E. Jenkins and A. V. Manohar, Phys. Lett. B **335**, 452 (1994).
[21] S. T. Hong and G. E. Brown, Nucl. Phys. **A580**, 408 (1994).
[22] M. A. Luty, J. March-Russell, and M. J. White, Phys. Rev. D **51**, 2332 (1995).
[23] M. K. Banerjee and J. Milana, Phys. Rev. D **54**, 5804 (1996).
[24] J. Linde and H. Snellman, Phys. Rev. D **53**, 2337 (1996); J. Linde, T. Ohlsson, and H. Snellman, Phys. Rev. D **57**, 5916 (1998).
[25] P. Ha, Phys. Rev. D **58**, 113003 (1998).
[26] J. Franklin, Phys. Rev. D **66**, 033010 (2002).
[27] C. Hayne and N. Isgur, Phys. Rev. D **25**, 1944 (1982).
[28] M. M. Giannini, Rep. Prog. Phys. **54**, 453 (1991).
[29] F. Schlumpf, Phys. Rev. D **48**, 4478 (1993).
[30] M. N. Butler, M. J. Savage, and R. P. Springer, Phys. Rev. D **49**, 3459 (1994).
[31] A. J. Buchmann, E. Hernandez, and A. Faessler, Phys. Rev. C **55**, 448 (1997); A. J. Buchmann, in *Baryons '98*, edited by D. W. Menze and B. Metsch (Word Scientific, Singapore, 1999), p. 731.
[32] F. X. Lee, Phys. Rev. D **57**, 1801 (1998); Phys. Lett. B **419**, 14 (1998).
[33] G. Wagner, A. J. Buchmann, and A. Faessler, J. Phys. G **26**, 267 (2000).
[34] T. M. Aliev, A. Ozpineci, and M. Savci, Nucl. Phys. **A678**, 443 (2000).
[35] B. O. Kerbikov, Phys. At. Nucl. **64**, 1856 (2001).
[36] S. Sahu, Rev. Mex. Fis. **48**, 48 (2002).
[37] H. Dahiya and M. Gupta, Phys. Rev. D **67**, 114015 (2003).
[38] B. Julia-Diaz and D. O. Riska, Nucl. Phys. **A739**, 69 (2004).
[39] G. S. Yang, H. C. Kim, M. Praszalowicz, and K. Goeke, Phys. Rev. D **70**, 114002 (2004).
[40] C. S. An, Q. B. Li, D. O. Riska, and B. S. Zou, Phys. Rev. C **74**, 055205 (2006); **75**, 069901(E) (2007).
[41] H. C. Kim and M. Praszalowicz, Phys. Lett. B **585**, 99 (2004); H. C. Kim, M. Praszalowicz, and K. Goeke, Phys. Rev. D **57**, 2859 (1998).
[42] A. I. Machavariani and A. Faessler, arXiv:0809.1303; arXiv:0804.1322.
[43] J. He and Y. B. Dong, Commun. Theor. Phys. **43**, 139 (2005).
[44] K. Hashimoto, T. Sakai, and S. Sugimoto, Prog. Theor. Phys. **120**, 1093 (2008).
[45] D. Arndt and B. C. Tiburzi, Phys. Rev. D **69**, 114503 (2004); **68**, 114503 (2003); **69**, 059904(E) (2004).
[46] M. D. Slaughter, arXiv:0911.4756.
[47] F. J. Jiang and B. C. Tiburzi, Phys. Rev. D **81**, 034017 (2010).
[48] K. Thakkar, B. Patel, A. Majethiya, and P. C. Vinodkumar, arXiv:1001.0849.
[49] L. S. Geng, J. Martin Camalich, and M. J. Vicente Vacas, Phys. Rev. D **80**, 034027 (2009).
[50] R. Flores-Mendieta, Phys. Rev. D **80**, 094014 (2009).

[51] G. Blanpied *et al.*, Phys. Rev. C **64**, 025203 (2001).
[52] C. Amsler *et al.* (Particle Data Group), Phys. Lett. B **667**, 1 (2008).
[53] B. Schwesinger and H. Weigel, Nucl. Phys. **A540**, 461 (1992).
[54] C. Gobbi, S. Boffi, and D. O. Riska, Nucl. Phys. **A547**, 633 (1992).
[55] R. K. Sahoo, A. R. Panda, and A. Nath, Phys. Rev. D **52**, 4099 (1995).
[56] N. Barik, P. Das, and A. R. Panda, Pramana **44**, 145 (1995).
[57] G. Dillon and G. Morpurgo, Phys. Lett. B **448**, 107 (1999).
[58] A. J. Buchmann and R. F. Lebed, Phys. Rev. D **62**, 096005 (2000).
[59] A. J. Buchmann and R. F. Lebed, Phys. Rev. D **67**, 016002 (2003).
[60] A. J. Buchmann, J. A. Hester, and R. F. Lebed, Phys. Rev. D **66**, 056002 (2002).
[61] A. J. Buchmann and E. M. Henley, Phys. Rev. D **65**, 073017 (2002);
[62] T. Ledwig, A. Silva, and M. Vanderhaeghen, Phys. Rev. D **79**, 094025 (2009).
[63] N. Isgur, G. Karl, and R. Koniuk, Phys. Rev. D **25**, 2394 (1982).
[64] D. Drechsel and M. M. Giannini, Phys. Lett. **143B**, 329 (1984).
[65] W. J. Leonard and W. J. Gerace, Phys. Rev. D **41**, 924 (1990).
[66] M. I. Krivoruchenko and M. M. Giannini, Phys. Rev. D **43**, 3763 (1991).
[67] J. Kroll and B. Schwesinger, Phys. Lett. B **334**, 287 (1994).
[68] A. J. Buchmann and E. M. Henley, Phys. Rev. C **63**, 015202 (2000).
[69] K. Azizi and K. Azizi, Eur. Phys. J. C **61**, 311 (2009).
[70] R. F. Lebed, Phys. Rev. D **51**, 5039 (1995).
[71] B. C. Tiburzi, Phys. Rev. D **71**, 054504 (2005).
[72] B. C. Tiburzi, Phys. Rev. D **79**, 077501 (2009).
[73] C. Alexandrou, T. Korzec, T. Leontiou, J. W. Negele, and A. Tsapalis, Proc. Sci., LATTICE2007 (2007) 149 [arXiv:0710.2744].
[74] C. Alexandrou *et al.*, Phys. Rev. D **79**, 014507 (2009).
[75] C. Alexandrou *et al.*, Nucl. Phys. **A825**, 115 (2009).
[76] S. Boinepalli, D. B. Leinweber, P. J. Moran, A. G. Williams, J. M. Zanotti, and J. B. Zhang, Phys. Rev. D **80**, 054505 (2009).
[77] C. W. Bernard, T. Draper, K. Olynyk, and M. Rushton, Phys. Rev. Lett. **49**, 1076 (1982).
[78] D. B. Leinweber, T. Draper, and R. M. Woloshyn, Phys. Rev. D **46**, 3067 (1992).
[79] F. X. Lee, R. Kelly, L. Zhou, and W. Wilcox, Phys. Lett. B **627**, 71 (2005).
[80] C. Aubin, K. Orginos, V. Pascalutsa, and M. Vanderhaeghen, Phys. Rev. D **79**, 051502(R) (2009).
[81] I. C. Cloet, D. B. Leinweber, and A. W. Thomas, Phys. Lett. B **563**, 157 (2003).
[82] G. Ramalho, M. T. Peña, and F. Gross, Phys. Lett. B **678**, 355 (2009).
[83] F. Gross, G. Ramalho, and M. T. Peña, Phys. Rev. C **77**, 015202 (2008).
[84] G. Ramalho, M. T. Peña, and F. Gross, Eur. Phys. J. A **36**, 329 (2008).
[85] G. Ramalho and M. T. Peña, Phys. Rev. D **80**, 013008 (2009).
[86] M. Burkardt, Int. J. Mod. Phys. A **18**, 173 (2003).
[87] C. E. Carlson and M. Vanderhaeghen, Phys. Rev. Lett. **100**, 032004 (2008).
[88] G. A. Miller and J. Arrington, Phys. Rev. C **78**, 032201 (2008).
[89] G. Ramalho, M. T. Peña, and A. Stadler (unpublished).
[90] V. Pascalutsa, M. Vanderhaeghen, and S. N. Yang, Phys. Rep. **437**, 125 (2007).
[91] C. Alexandrou and G. Koutsou, Phys. Rev. D **78**, 094506 (2008).
[92] F. Gross, G. Ramalho, and M. T. Peña, Phys. Rev. C **77**, 035203 (2008).
[93] G. Ramalho and M. T. Peña, J. Phys. G **36**, 115011 (2009).
[94] S. Nozawa and D. B. Leinweber, Phys. Rev. D **42**, 3567 (1990).
[95] M. Benmerrouche, R. M. Davidson, and N. C. Mukhopadhyay, Phys. Rev. C **39**, 2339 (1989).
[96] H. Haberzettl, arXiv:nucl-th/9812043.
[97] F. Gross and P. Agbakpe, Phys. Rev. C **73**, 015203 (2006).
[98] C. Alexandrou, G. Koutsou, H. Neff, J. W. Negele, W. Schroers, and A. Tsapalis, Phys. Rev. D **77**, 085012 (2008).
[99] C. Alexandrou (private communication).
[100] A. W. Thomas, Adv. Nucl. Phys. **13**, 1 (1984).
[101] E. J. Hackett-Jones, D. B. Leinweber, and A. W. Thomas, Phys. Lett. B **494**, 89 (2000).
[102] S. Boinepalli, D. B. Leinweber, A. G. Williams, J. M. Zanotti, and J. B. Zhang, Phys. Rev. D **74**, 093005 (2006).
[103] C. Alexandrou, G. Koutsou, J. W. Negele, and A. Tsapalis, Phys. Rev. D **74**, 034508 (2006).
[104] M. Gockeler, T. R. Hemmert, R. Horsley, D. Pleiter, P. E. L. Rakow, A. Schafer, and G. Schierholz (QCDSF Collaboration), Phys. Rev. D **71**, 034508 (2005).
[105] R. D. Young, D. B. Leinweber, and A. W. Thomas, Nucl. Phys. B, Proc. Suppl. **128**, 227 (2004); D. B. Leinweber, A. W. Thomas, A. G. Williams, R. D. Young, J. M. Zanotti, and J. B. Zhang, Nucl. Phys. **A737**, 177 (2004).
[106] J. M. Richard and P. Taxil, Z. Phys. C **26**, 421 (1984).
[107] K. Tsushima and G. Ramalho (unpublished).
[108] F. Gross, G. Ramalho, and K. Tsushima, Phys. Lett. B **690**, 183 (2010).
[109] G. Ramalho, K. Tsushima, and F. Gross, Phys. Rev. D **80**, 033004 (2009).
[110] C. Alexandrou, T. Korzec, G. Koutsou, and Y. Proestos, Proc. Sci., LAT2009 (2009) 155 [arXiv:0910.3471].